J. Fluid Mech. (1991), *vol.* 228, *pp.* 661–691
Printed in Great Britain

Splitting, merging and wavelength selection of vortices in curved and/or rotating channel flow due to Eckhaus instability

By Y. GUO AND W. H. FINLAY
Department of Mechanical Engineering, University of Alberta, Edmonton, Alberta, Canada T6G 2G8

(Received 14 June 1990 and in revised form 10 January 1991)

In channels with rotation (about their spanwise axis) or curvature or both, steady two-dimensional vortices develop above a critical Reynolds number Re_c, owing to centrifugal or Coriolis effects. The stability of these streamwise oriented roll cells to two-dimensional, spanwise-periodic perturbations (i.e. Eckhaus stability) is examined numerically using linear stability theory and spectral methods. The results are then confirmed by nonlinear flow simulations. In channels with curvature or rotation or both, the Eckhaus stability boundary is found to be a small closed loop. Within the boundary, two-dimensional vortices are stable to spanwise perturbations. Outside the boundary, Eckhaus instability is found to cause the vortex pairs to split apart or merge together. For all channels examined, two-dimensional vortices are always unstable when $Re > 1.7\,Re_c$. Usually, the most unstable spanwise perturbations are subharmonic disturbances, which cause two pairs of vortices with small wavenumbers to be split apart by the formation of a new vortex pair, but cause two pairs of vortices with large wavenumber to merge into a single pair. Recent experimental observations of splitting and merging of vortex pairs are discussed. When Re is not too high ($Re < 4.0\,Re_c$), the wavenumbers of vortices are selected by Eckhaus instability and most experimentally observed wavenumbers are close to the ones that are least unstable to spanwise perturbations.

1. Introduction

As the Reynolds number, Re, is increased, the flow in channels with either curvature or rotation or both undergoes a supercritical transition from spanwise uniform one-dimensional Poiseuille type flow to a state with spanwise periodicity containing two-dimensional streamwise-oriented vortices. This transition is characterized by the one-dimensional flow losing its stability to spanwise perturbations, owing to an imbalance of centrifugal, Coriolis and pressure forces. For fixed curvature or rotation rate, the transition occurs when Re exceeds some critical value Re_c. When $Re = Re_c$, there is only one possible spanwise wavenumber α_c for the two-dimensional vortices (cf. Tritton & Davies 1985; Finlay, Keller & Ferziger 1988; Alfredsson & Persson 1989; Finlay 1990 for a literature review on the primary instability of one-dimensional Poiseuille type flow to two-dimensional vortices in channels with either curvature or rotation, and Matsson & Alfredsson 1990 for channels with both curvature and rotation). At higher Re, a continuous band of stable wavenumbers for the two-dimensional vortices is expected. The limits of this band are given by several different instabilities of the two-dimensional vortices. For channels with infinite

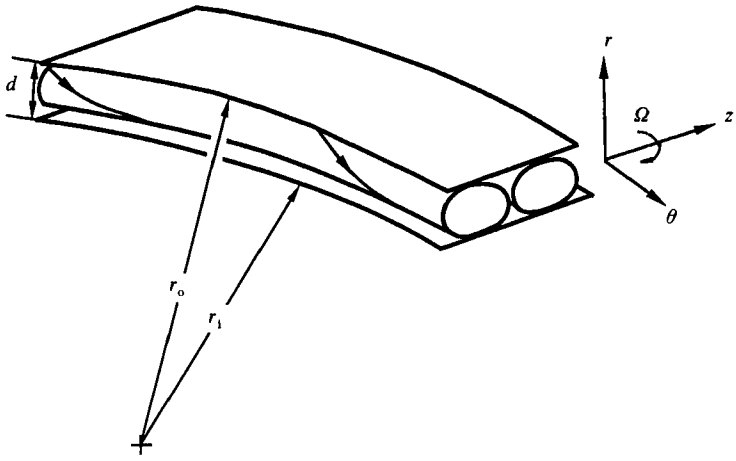

FIGURE 1. The geometry of curved and/or rotating channel is shown. The flow is periodic in z.

span, one of the most important instabilities of the two-dimensional vortices is due to spanwise perturbations. In this paper, linear stability theory and flow simulation are used to examine this type of instability numerically for the flow in channels with curvature or rotation or both.

The channel geometry is given in figure 1. The channel spacing is $d = r_o - r_i$. The streamwise and spanwise directions of the flow are given by θ and z. The Reynolds number is $Re = \bar{U}d/2\nu$, where $\bar{U}$ is the mean (bulk) streamwise velocity. The radius ratio of the two walls is $\eta = r_i/r_o$. The rotation number is defined as $Ro = \Omega d/2\nu$, where Ω is the rotation speed of the system about the z-axis. The term rotating channel will be used to mean $Ro \neq 0$ and $\eta = 1.0$, while the term curved channel refers to $Ro = 0$ and $\eta < 1.0$. Otherwise the channel has both curvature and rotation. The spanwise wavenumber of the vortices is defined as $\alpha = \pi d/\lambda$, where λ is the spanwise vortex spacing. The term 'two-dimensional vortices' indicates that each velocity component depends only on the two directions r and z. The flow is three-dimensional in the sense of having three velocity components. In channel flow experiments, the spanwise dimension of the channel is h and the aspect ratio $\Gamma = h/d$ is a finite number.

Instabilities induced by centrifugal and Coriolis forces have been studied for many years. One classical example is Taylor–Couette flow. Years of effort by many researchers (cf. DiPrima & Swinney 1985) has led to considerable knowledge about the physics of the transition to turbulence in this geometry. Similar work is needed for the flow in channels with curvature or rotation or both. A better understanding of transition in these channel geometries may lead us to a better understanding of many flows including the flow inside impellers of centrifugal pumps or compressors, coolant flow in turbine blades, and deep-sea currents partitioned by submarine ridges.

There has been some work done on the instabilities of two-dimensional vortices in channels with either curvature or rotation or both. Recently, Finlay *et al.* (1988) and Finlay (1990) have examined numerically the instability with respect to perturbations that cause the vortices to become wavy in the streamwise direction. This instability does not restrict the spanwise wavenumber of the flow. These wavy vortices are similar to oscillatory Rayleigh–Bénard convection or wavy Taylor vortices. Though the flow in channels with either curvature or rotation or both bears

some similarity to Taylor–Couette flow, recent experimental studies in channels with large aspect ratio ($\Gamma \geqslant 40$) show there is considerable unsteadiness that is not present in Taylor vortex flow (cf. Ligrani & Niver 1988 for the curved channel; Alfredsson & Persson 1989 for the rotating channel; Matsson & Alfredsson 1990 for the curved-rotating channel). When viewed in a spanwise–streamwise plane, the vortices cause long streaks in experimental flow visualizations. These streaks are occasionally split apart by new streaks or merge together (Alfredsson & Persson 1989; Matsson & Alfredsson 1990). In this paper we will refer to these phenomena as the splitting and merging of vortex pairs. These terms are always used to describe the behaviour of two or more vortex pairs, not individual vortex tubes. In the curved channel, spanwise motion, modulation and oscillation of vortices are also observed (Ligrani & Niver 1988). These phenomena are not well understood. Studies on the instability of two-dimensional vortices to spanwise perturbations in Rayleigh–Bénard convection and Taylor–Couette flow show that an Eckhaus instability restricts the band of stable wavenumbers (Clever & Busse 1974; Riecke & Paap 1986). For Taylor vortices good agreement exists between theoretical and experimental results for the band of stable wavenumbers (Riecke & Paap 1986; Dominguez-Lerma, Cannell & Ahler 1986). If vortices are created with wavenumber outside the stable region, Eckhaus instability causes the vortices to change their wavelength so that it lies in the stable region. But in channels with either curvature or rotation or both, little of such work has been done.

The instability with respect to spanwise perturbations bears the name of Eckhaus, since the first study of this type of instability was done by Eckhaus (1965, Eckhaus' work first appeared in 1963 in French in *Journal de Physique*) for Tollmien–Schlichting waves, using an amplitude expansion method. His result shows that for a system of real eigenvalues and parameters, the band of stable wavenumbers α is given by $(\alpha_c-\alpha_-)/\sqrt{3} < \alpha-\alpha_c < (\alpha_+-\alpha_c)/\sqrt{3}$, where α_- and α_+ are the wavenumbers on each branch of the neutral curve of primary instability for a given Re. The Eckhaus criterion has been proven valid in Rayleigh–Bénard convection and Taylor–Couette flow for Re close to Re_c. Stuart & DiPrima (1978) have corrected the above criterion for a general periodic flow and demonstrated the equivalence between the Eckhaus instability and the sideband instability of Benjamin & Feir (1967). To our knowledge, the stability criterion they give is the only available criterion for the flow in curved and/or rotating channels. However, this criterion is only valid in the region close to Re_c.

At low Re in curved and/or rotating channels, the wavenumbers of experimentally observed vortices are close to those with the maximum growth rate of primary instability (the maximum primary growth rate, cf. Finlay *et al.* 1988; Alfredsson & Persson 1989; Ligrani & Niver 1988). This suggests that perturbations with these wavenumbers develop faster than others from the one-dimensional flow, thus becoming the dominant wavenumbers in the fully developed vortex flow. This is the only available comment in the literature regarding a mechanism for spanwise wavenumber selection in channels with either curvature or rotation. Yet this comment does not apply to high Re where the observed wavenumbers are considerably smaller than those with maximum primary growth rate (Finlay *et al.* 1988; Alfredsson & Persson 1989; Ligrani & Niver 1988).

In this paper, the Eckhaus instability of the flow in channels with either curvature or rotation or both is studied. The formulation of the problem and numerical method we use are briefly described in §2. In §3, we present Eckhaus boundaries for channels with either curvature or rotation or both. We discuss the splitting and merging of

vortices in §4. A spanwise wavenumber selection mechanism is discussed in §5 and recurrent splitting and merging in § 6. Nonlinear flow simulations of splitting, merging and wavelength selection are given §7.

2. Theory and numerical method

For steady, two-dimensional, streamwise-oriented vortices, the pressure gradient ∇p is a constant and the velocity of the flow can be represented by

$$\boldsymbol{u}^0 = \left(-\frac{1}{r}\frac{\partial \psi}{\partial z}, u_\theta, \frac{1}{r}\frac{\partial \psi}{\partial r}\right), \tag{2.1}$$

where ψ is the stream function. The governing equations are the incompressible, steady, Navier–Stokes equations:

$$\left.\begin{aligned} \boldsymbol{u}^0 \cdot \nabla \boldsymbol{u}^0 &= -\frac{1}{\rho}\nabla p + \nu \nabla^2 \boldsymbol{u}^0 - 2\Omega \boldsymbol{e}_z \times \boldsymbol{u}^0, \\ \nabla \cdot \boldsymbol{u}^0 &= 0. \end{aligned}\right\} \tag{2.2}$$

Periodic boundary conditions are imposed in the z-direction, since the flow is assumed to have infinite span. Spectral methods are used to solve the above equations. We use a Fourier Galerkin method in the z-direction and a Chebyshev tau method in the r-direction. To eliminate aliasing error, the $\frac{3}{2}$ rule is used to evaluate the nonlinear terms (cf. Canuto *et al.* 1988). Adequate resolution is insured by monitoring the energies in the highest modes. In our computation, the numbers of Fourier modes N and Chebyshev modes M vary from 16×16 to 20×26 ($N \times M$) depending on Re, η, Ro and the spanwise wavenumber α of the vortices. Normally we include only one pair of vortices in the computational box.

Once the two-dimensional vortex flow $\boldsymbol{u}^0$ is found, its stability can be examined using linear stability analysis. For small disturbances $\boldsymbol{u}'$, the perturbation equation can be linearized as

$$\left.\begin{aligned} \frac{\partial \boldsymbol{u}'}{\partial t} + \boldsymbol{u}^0 \cdot \nabla \boldsymbol{u}' + \boldsymbol{u}' \cdot \nabla \boldsymbol{u}^0 &= -\frac{1}{\rho}\nabla p' + \nu \nabla^2 \boldsymbol{u}' - 2\Omega \boldsymbol{e}_z \times \boldsymbol{u}', \\ \nabla \cdot \boldsymbol{u}' &= 0. \end{aligned}\right\} \tag{2.3}$$

In general the perturbation $\boldsymbol{u}'$ can be expressed as

$$\boldsymbol{u}'(r, \theta, z) = \tilde{\boldsymbol{u}}(r, z) \exp\left[st + \mathrm{i}(\mathrm{d}\theta + bz)\right], \tag{2.4}$$

where d and b are the streamwise and spanwise wavenumbers of the perturbation. Since we are only interested in the spanwise perturbation, we set $d = 0$. Inserting the above expression into (2.3), the stability problem becomes an eigenvalue problem: the stability of $\boldsymbol{u}^0$ is determined by σ, the real part of the eigenvalue $s = \sigma + \mathrm{i}\omega$. The flow pattern of the perturbation is given by

$$\mathrm{Re}\{\tilde{\boldsymbol{u}}(r, z) \exp(\mathrm{i}bz)\}. \tag{2.5}$$

Fourier Galerkin and Chebyshev tau spectral methods are used to solve the above eigenvalue problem. To reduce the number of unknown variables, the following representation of the perturbation is used:

$$\boldsymbol{u}' = \nabla \times \varphi \boldsymbol{e}_r + \tfrac{1}{2}(1-\eta)\nabla \times \nabla \times \chi \boldsymbol{e}_r. \tag{2.6}$$

Equation (2.3) then is reduced to two scalar equations: $\boldsymbol{e}_r \cdot \nabla \times (2.3)$ and $\boldsymbol{e}_r \cdot \nabla \times \nabla \times (2.3)$. If the resolution of $\boldsymbol{u}^0$ is $N \times M$, the dimension of the resulting complex eigenvalue problem is $2 \times (M-2)(N+1)$, compared with $(M-1)(\frac{1}{2}N+1)+(M-3)(\frac{1}{2}N)$ for the wavy type instability where only the out-phase (or in-phase) modes are needed (Finlay *et al.* 1988; Jones 1981, 1985). Computation of the Eckhaus instability is thus much more expensive than in the wavy instability, especially when $N \times M$ is large. Among $2 \times (M-2)(N+1)$ eigenvalues, we are only interested in the eigenvalue with the largest real part. We will use the term 'Eckhaus eigenvalue' to refer to this eigenvalue and 'Eckhaus growth rate' to refer to the real part of this eigenvalue. A similar method for solving the eigenvalue problem was used successfully by Clever & Busse (1974) for Rayleigh–Bénard convection and by Nagata (1986, 1988) and Jones (1985) for Taylor–Couette flows. More details of this method can be found in their papers.

To avoid a singularity when $\eta = 1.0$ the non-dimensional variables must be chosen carefully. The following non-dimensional variables (x, y, z, t) are used in our formulation:

$$r/r_0 = \tfrac{1}{2}(1+\eta)+\tfrac{1}{2}(1-\eta)\,x,$$

$$\theta = \tfrac{1}{2}(1-\eta)\,y,$$

$$z^*/r_0 = \frac{1}{2\alpha}(1-\eta)\,z,$$

$$t^* = \frac{d^2}{4\nu}t,$$

where z^* and t^* are dimensional, $-1.0 \leqslant x \leqslant 1.0$ and $0 \leqslant z \leqslant 2\pi$. The perturbation wavenumber b is thus non-dimensionalized by the spanwise wavenumber of the vortices $2\pi/\lambda$. The resulting codes were extensively verified by duplicating the results of previous authors, including the Eckhaus boundary for Taylor vortices obtained by Riecke & Paap (1986), the wavy instability ($b = 0$, $d \neq 0$) results for Taylor vortices obtained by Jones (1985), and the wavy instability results obtained in channel flows with curvature or rotation by Finlay *et al.* (1988) and Finlay (1990).

It has been reported (Zebib 1984; Gardner, Trogdon & Douglass 1989) that the Chebyshev tau method produces spurious eigenvalues and in some cases it is difficult to distinguish true eigenvalues from spurious ones. In our problem, spurious eigenvalues are also found. However, because only one spurious eigenvalue with a positive real part is produced by the Chebyshev tau method for each Fourier mode and these spurious eigenvalues always have much larger magnitude ($|s|$) than the true eigenvalues (cf. Fox & Parker 1968), it is not difficult to distinguish between the true and spurious eigenvalues. The spurious eigenvalues can also be found easily by changing the number of modes used, i.e. M and N; this causes the spurious eigenvalues to change drastically whereas the true eigenvalues vary little with M and N for sufficiently large M and N.

It can be shown that for any spanwise periodic flow, the eigenvalue $s = \sigma + \mathrm{i}\omega$ and the non-dimensional spanwise perturbation wavenumber b have the following relation:

$$s(b) = s(\pm k \pm b), \tag{2.7}$$

where $0 < b < 1.0$ and $k = 1, 2, 3, \ldots$. This result reduces the values of b we need examine to $0 < b < \frac{1}{2}$, since setting $k = 1$ shows that $s(b) = s(1-b)$ (i.e. s is symmetric about $b = \frac{1}{2}$) and setting $k = 2, 3, 4, \ldots$, covers the remaining b.

Equation (2.7) applies for any spanwise periodic flow. Our numerical results verify (2.7) for both Taylor–Couette flow and the flow in channels with either curvature or rotation or both. The numerical results given by Nagata & Busse (1983, their figure 10) and by Paap & Riecke (1990, their figure 2) also demonstrate the symmetry property of σ about $b = 0.5$ for $0 < b < 1$ in buoyancy driven shear-layer flow and Taylor–Couette flow. It seems some previous researchers were not aware of this property. Its immediate significance is to drastically reduce the range of perturbation wavenumbers that need to be explored and thus to reduce computational expense. In our studies, since the numerical difference between the eigenvalues s for $0 < b < 0.5$ and $0.5 < b < 1.0$ is less than 0.1% for the stated resolution, we only calculate s for $0 < b < 0.5$. The values of s for $0.5 < b < 1.0$ are obtained from the symmetry property in (2.7).

3. Eckhaus stability boundary

The Eckhaus stability boundary is determined by a sign change in the Eckhaus growth rate σ as the parameters of the system are varied. Within the Eckhaus boundary, the Eckhaus growth rate is always negative. In the region neighbouring the Eckhaus boundary, our numerical results show the eigenvalue with the maximum Eckhaus growth rate is always real. The stability boundary is thus determined by non-oscillatory perturbations. Figure 2 shows the Eckhaus boundaries for several channels with either curvature or rotation or both. In a curved channel ($\eta = 0.975$) with rotation, Matsson & Alfredsson (1990) find the primary instability occurs as a Hopf bifurcation when $-0.014 > Ro > -0.0164$. Thus for Ro in this range there are no steady two-dimensional vortex solutions. The two cases we present in figure 2 (*c*) at $Ro = -0.0125$ and -0.02 are just outside the range of Ro for the primary instability to appear as a Hopf bifurcation. Figure 2 shows that the Eckhaus stable region for the flow in curved and/or rotating channels is a small closed region tangent to the minimum of the neutral stability curve for the primary instability. In all cases calculated by us, the Eckhaus boundary is only a weak function of η and Ro.

When compared to other spanwise periodic flows known to the authors, channel flows with either curvature or rotation or both exhibit significant differences. For example in Taylor–Couette flow, the Eckhaus boundary is an open region, i.e. for any Re, there is always a band of stable wavenumber α. On the Eckhaus boundary, the spanwise wavenumber of perturbations, b, approaches zero when Re is not very high (Riecke & Paap 1986). When Re is high, the boundary is given by $b = 0.5$ (Paap & Riecke 1990). Paap & Riecke (1990) refer to this as a short-wavelength instability, in order to distinguish it from the long-wavelength nature of the classical Eckhaus instability. Numerical calculations done by us for Taylor–Couette flow show that as α moves away from the Eckhaus boundary, b approaches 0.5 when Re is not very high. As Re increases, this happens very quickly. This is consistent with the results given by Paap & Riecke (1990). Our results also show that for any Re, α and b, the eigenvalue with maximum real part is always real in the Taylor–Couette problem. All parameters of the system are thus real and the Eckhaus stability criterion given by Eckhaus (1965) is valid in the region near Re_c (Riecke & Paap 1986).

In channels with either curvature or rotation or both, the situation is much more complicated. We have studied the case of the curved channel with $\eta = 0.975$ most carefully. Our results show that near the left-hand side of the Eckhaus boundary, the eigenvalue with Eckhaus growth rate is real for any b. Figure 3 shows $\sigma(b)$ at $Re = 1.07\,Re_c$ (figure 3*a*) and $1.225\,Re_c$ (figure 3*b*) as α approaches the left-hand side of the

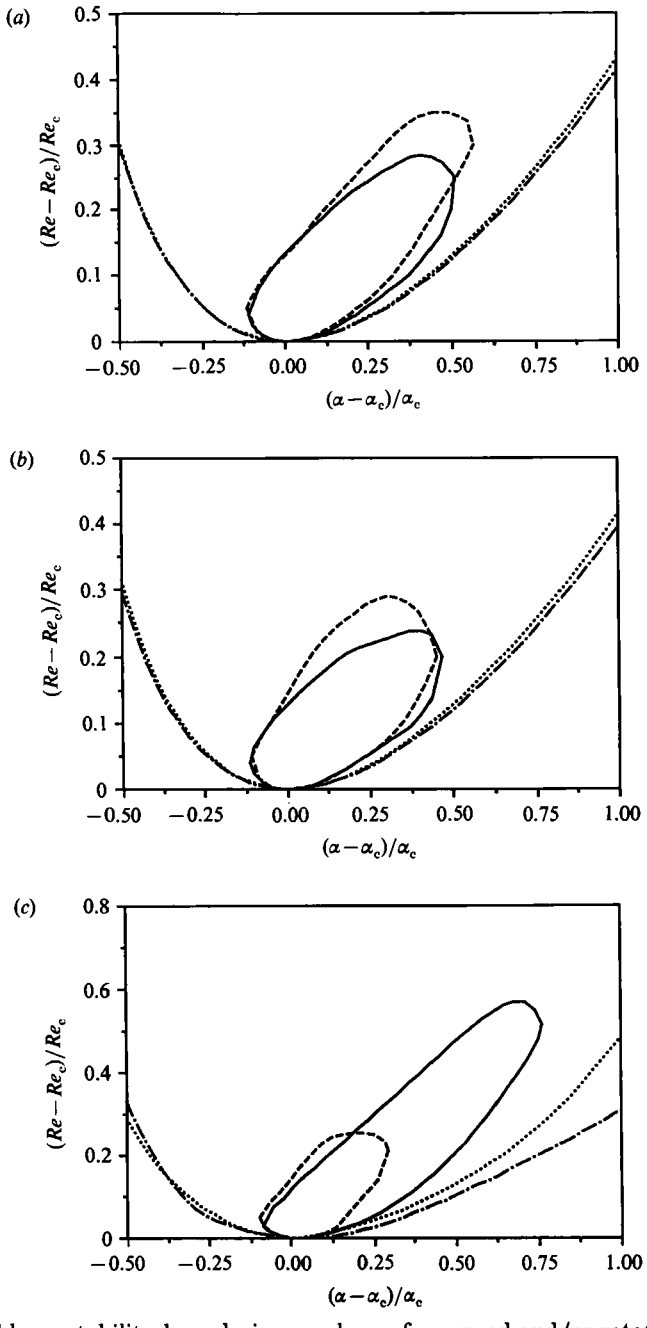

FIGURE 2. Eckhaus stability boundaries are shown for curved and/or rotating channel flow. The primary stability boundary is included for reference. (*a*) Shown for curved channels are Eckhaus: ——, $\eta = 0.975$ ($Re_c = 114.26, \alpha_c = 1.98$); – – –, $\eta = 0.7$ ($Re_c = 35.83, \alpha_c = 2.07$); and primary: —·—, $\eta = 0.975$; -----, $\eta = 0.7$. (*b*) Shown for rotating channels are Eckhaus: ——, $Ro = 0.005$ ($Re_c = 198.95, \alpha_c = 2.01$); – – –, $Ro = 0.25$ ($Re_c = 44.30, \alpha_c = 2.46$); and primary: —·—, $Ro = 0.005$; -----, $Ro = 0.25$. (*c*) Shown for curved-rotating channels are Eckhaus: ——, $\eta = 0.975, Ro = -0.0125$ ($Re_c = 275.4, \alpha_c = 1.96$); – – –, $\eta = 0.975, Ro = -0.02$ ($Re_c = 195.0, \alpha_c = 2.16$); and primary: —·—, $\eta = 0.975, Ro = -0.0125$; -----, $\eta = 0.975, Ro = -0.02$.

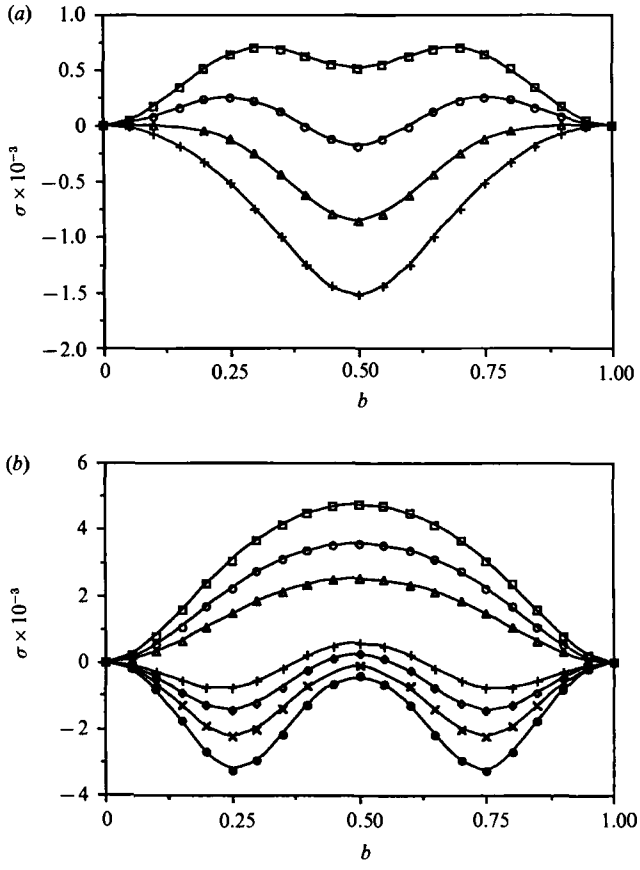

FIGURE 3. Eckhaus growth rate σ as a function of spanwise perturbation wavenumber b in a curved channel ($\eta = 0.975$) as the spanwise wavenumber α of two-dimensional vortices approaches the left-hand side of the Eckhaus boundary (α_{left}) at (*a*) $Re = 1.07Re_c$ and (*b*) $Re = 1.225Re_c$. In (*a*): $\alpha_{\text{left}} = 1.8$; □, $\alpha = 1.7$; ○, $\alpha = 1.75$; △, $\alpha = 1.8$; +, $\alpha = 1.85$. In (*b*): $\alpha_{\text{left}} = 2.355$; □, $\alpha = 1.6$; ○, $\alpha = 1.8$; △, $\alpha = 2.0$; +, $\alpha = 2.3$; ◇, $\alpha = 2.35$; ×, $\alpha = 2.4$; ●, $\alpha = 2.45$.

Eckhaus boundary. Figure 3(*a*) shows that at $Re = 1.07\ Re_c$, $b = 0$ determines the Eckhaus boundary. Figure 3(*b*), however, shows that at $Re = 1.225\ Re_c$, $b = 0.5$ determines the boundary.

In the neighbourhood of the right-hand side of the Eckhaus boundary, the eigenvalue with Eckhaus growth rate is not real for all b when $Re > 1.1Re_c$. For some b, a complex conjugate pair has the maximum real part. Figure 4 shows the eigenvalues $s(b)$ for various α near the right-hand side of the Eckhaus boundary at $Re = 1.07Re_c$ (figure 4*a*) and $Re = 1.225Re_c$ (figure 4*b*). The eigenvalue has zero imaginary part at $Re = 1.07Re_c$ so only $\sigma(b)$ is shown in figure 4(*a*). In figure 4(*b*) only the positive imaginary part of the eigenvalue is shown. By using different numbers of Chebyshev modes and Fourier modes, we have verified that these complex eigenvalues are not spurious eigenvalues produced by the Chebyshev tau method. Figure 4(*a*) shows that at $Re = 1.07Re_c$, $b = 0.25$ on the boundary. Figure 4(*b*) shows that at $Re = 1.225Re_c$, $b = 0.5$ on the boundary. Figure 4 also shows that the imaginary part of the eigenvalue which determines the Eckhaus boundary is zero on the boundary.

The value of $b(Re)$ on the boundary is shown in figure 5. On both sides of the

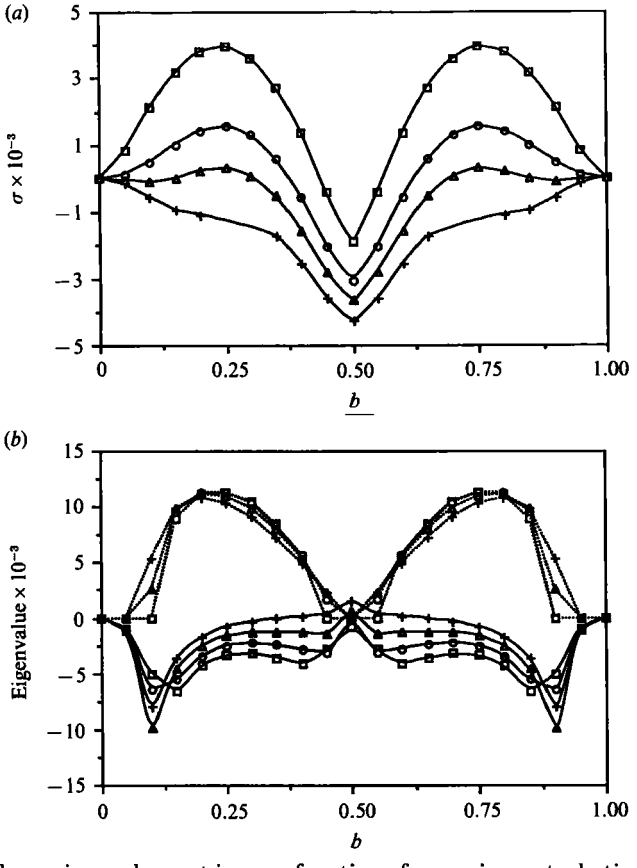

FIGURE 4. Eckhaus eigenvalue, $\sigma + i\omega$, as a function of spanwise perturbation wavenumber b as the spanwise wavenumber α of two-dimensional vortices approaches the right-hand side of the Eckhaus boundary (α_{right}) at (*a*) Re = $1.07Re_c$ and (*b*) $Re = 1.225Re_c$. In (*a*), $\omega(b) = 0$; $\alpha_{right} = 2.565$; +, $\alpha = 2.55$; △, $\alpha = 2.575$; ○, $\alpha = 2.6$; □, $\alpha = 2.65$. In (*b*), $\alpha_{right} = 2.98$; □, $\alpha = 2.9$; ○, $\alpha = 2.95$; △, $\alpha = 3.0$; +, $\alpha = 3.05$; —— for σ; ----- for ω.

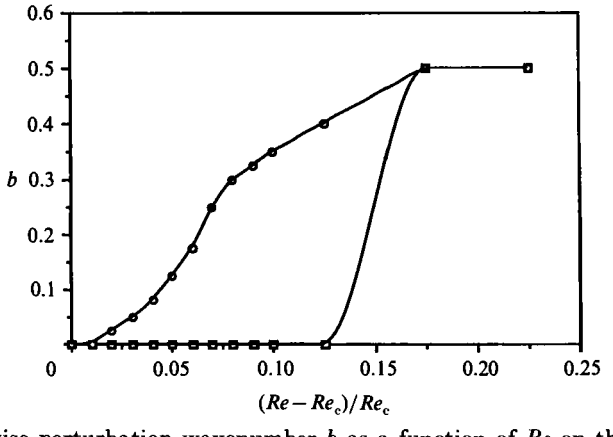

FIGURE 5. Spanwise perturbation wavenumber b as a function of Re on the Eckhaus boundary in a curved channel ($\eta = 0.975$): □, left-hand side of the Eckhaus boundary; ○, right-hand side of the boundary.

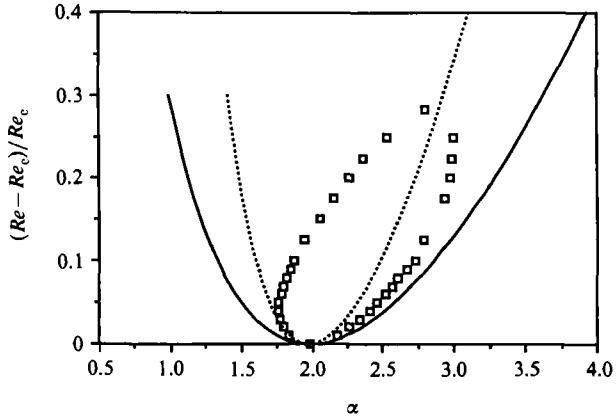

FIGURE 6. -----, stability criterion of Eckhaus (1965); ——, the primary stability boundary of Finlay *et al.* (1988) and □, the Eckhaus stability boundary in a curved channel with $\eta = 0.975$.

boundary, b reaches 0.5 when $Re \geqslant 1.175Re_c$. Clearly here the boundary defined by the instability of two-dimensional vortices to spanwise perturbations is not the classical Eckhaus stability boundary ($b \to 0$) found in Taylor–Couette flow. When $Re \leqslant 1.125Re_c$, only the left-hand side of the boundary is of the classical Eckhaus type. For simplicity, we still call the entire boundary an Eckhaus boundary. Figure 6 shows a comparison of the Eckhaus criterion (Eckhaus 1965), primary stability boundary (Finlay *et al.* 1988) and the Eckhaus boundary we have determined, all for a curved channel with $\eta = 0.975$. The Eckhaus stability criterion does not apply to the right-hand side of the Eckhaus boundary even in the region close to Re_c. On the left-hand side, it is valid with reasonable accuracy up to $Re < 1.04Re_c$. In Taylor–Couette flow, the Eckhaus stability criterion is valid with reasonable accuracy up to $1.1Re_c$ for both sides of the boundary (Riecke & Paap 1986). We believe that $b \neq 0$ and non-real eigenvalues on the right-hand side of the boundary are the reason why the Eckhaus criterion is not valid here. (Another case where the Eckhaus criterion does not apply is the inclined shear layer driven by wall heating (Nagata & Busse 1983). There, the Eckhaus criterion is invalid on both sides of the Eckhaus boundary even near Re_c). Although the perturbation equations for both Taylor–Couette flow and curved and/or rotating channel flow have the same form (2.3), the base flow $\boldsymbol{u}^0$ is not the same. In channel flow, the streamwise component of $\boldsymbol{u}^0$ decreases to zero away from a maximum near the centre of the channel, whereas in Taylor–Couette flow, the streamwise velocity is maximum at a wall. We believe this may be responsible for the difference between the Eckhaus instabilities in these geometries.

Beyond the top of the Eckhaus boundary, if Re/Re_c is not too high and α is not too small or too large, the eigenvalue with the maximum Eckhaus growth rate is given by $b = 0.5$ and is real. In the curved channel with $\eta = 0.975$, we find the eigenvalue with the maximum Eckhaus growth rate is entirely real in the region of $Re \leqslant 3.5Re_c$ and $1.8 \leqslant \alpha \leqslant 5.0$. But at given Re there does exist a spanwise wavenumber α' such that when $\alpha > \alpha'$, Eckhaus eigenvalues are complex for some $b \neq 0.5$. For example, at $Re = 2.0Re_c$, $\alpha' = 3.5$.

When Re/Re_c is very high, for example $Re/Re_c > 3.2$ in rotating channels, the real part of a complex conjugate pair is the largest for some α and so the corresponding perturbation is oscillatory. For example, at $Re = 472.5$ ($Re/Re_c = 5.56$) in the rotating channel $Ro = 0.03$, we find that when $2.0 \leqslant \alpha \leqslant 3.0$, an oscillatory unstable

mode has the largest σ, but for $\alpha \leqslant 2.0$ and $\alpha \geqslant 3.75$ the most unstable mode has zero imaginary part. Because the Eckhaus instability is probably less important at high Re than the wavy instability, and the computation becomes very expensive, only a few high Re cases have been explored. More work needs to be done before this type of oscillatory unstable mode can be understood.

Results similar to those discussed above were found in all channels that we examined. In all cases, two-dimensional vortices are unstable to spanwise perturbations when $Re > 1.7Re_c$ (they are often unstable at even lower Re). Since the Eckhaus stable region is small and most experiments have been done outside this region, the instability associated with the most unstable mode, which usually has $b = 0.5$, is an important instability in channel flows with curvature or rotation or both.

4. Splitting and merging of vortices

In channel flow experiments, vortex pairs are sometimes observed to merge together (reducing the number of vortices across the channel) or to be split apart by the formation of new vortex pairs (Ligrani & Niver 1988; Alfredsson & Persson 1989; Matsson & Alfredsson 1990). In some cases, the merging and splitting of vortex pairs happens repetitively (Ligrani, Kendall & Longest 1990). Similar phenomena have also been reported by Finlay *et al.* (1988), Finlay (1990) and Bland & Finlay (1991) in their numerical simulations of channel flows with curvature or rotation. We believe that the splitting and merging of vortex pairs are associated with the instability of two-dimensional vortices to spanwise perturbations. In §3 our linear stability results indicate that no two-dimensional vortex flow is stable to spanwise perturbations when $Re > 1.7Re_c$. In order to understand how these two-dimensional vortex pairs lose their stability to spanwise perturbations and split apart or merge together, we examine the flow pattern of the most unstable mode of linear stability theory. The flow pattern of the most unstable mode is given by the eigenfunction (2.5), which has the largest growth rate σ. It grows at the rate exp (σt).

4.1. *Taylor–Couette flow*

First, Taylor vortex flows are studied, because here linear stability theory calculations (Riecke & Paap 1986) and experimental observation (Dominguez-Lerma *et al.* 1986) of the Eckhaus boundary show good agreement. The pairing of vortices has been discussed by Paap & Riecke (1990) using bifurcation diagrams. Here we will discuss the splitting and merging of vortex pairs from the perspective of the flow patterns of the most unstable modes.

As mentioned before, as α moves away from the Eckhaus boundary in Taylor vortex flow, the value of b corresponding to the maximum Eckhaus growth rate increases from 0 to 0.5. Figures 7 and 8 show the Taylor vortices (figures 7*a*, 8*a*), their most unstable modes (figures 7*b*, 8*b*) and linear superpositions of these two (figures 7*c*, 8*c*, 8*d*) at $Re = 2.0Re_c$ outside each side of the Eckhaus boundary, where the maximum Eckhaus growth rate is given by $b = 0.5$ (the Eckhaus boundary has $\alpha_{\text{left}} = 1.188$, $\alpha_{\text{right}} = 2.425$). In figures 7(*a*) and 8(*a*), the centres of the Taylor vortex pairs are at $z/\lambda = 0$, 1.0 and 2.0, where the fluid flows from the convex wall to the concave wall (the outflow region). The streamwise direction is out of the plane of the plot. In figure 7(*b*), the unstable mode has three pairs of vortices in the space of two pairs of base vortices. If the perturbation maintains this character in the nonlinear state, one extra pair of vortices would be produced out of every two base pairs. Figure 7(*c*) is

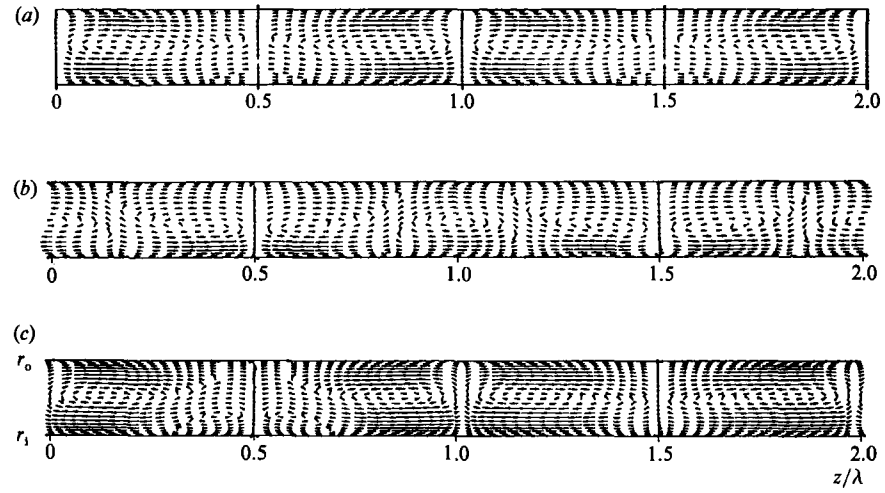

FIGURE 7. (*a*) Taylor vortices, (*b*) their most unstable mode, and (*c*) Taylor vortices + the most unstable mode, projected onto the (r, z)-plane at $Re = 2.0Re_c$, $\eta = 0.75$ and $\alpha = 1.17$, outside the left-hand side of the Eckhaus boundary ($\alpha_{\text{left}} = 1.188$). In (*c*), the kinetic energy of the most unstable mode is 1.4% of the base flow's kinetic energy. $b = 0.5$ for the most unstable mode.

a plot of the base flow (figure 7*a*) superimposed with the most unstable eigenfunction (figure 7*b*). The kinetic energy of the eigenfunction in figure 7 (*c*) has been set to 1.4% of the base flow's kinetic energy. A new pair of vortices is seen at $z/\lambda = 0.5$ near the convex wall that splits apart the pairs of vortices on either side of $z/\lambda = 0.5$ in the base flow. This indicates that splitting of vortices occurs upon exiting the left-hand side of the Eckhaus boundary. Outside the right-hand side of the Eckhaus boundary (figure 8*b*), one vortex pair of the unstable mode takes the space of two pairs of the base flow (except for small weak secondary vortices near the walls). Figure 8 (*c*) shows the most unstable eigenfunction (figure 8*b*) superimposed on the base flow (figure 8*a*). The kinetic energy of the perturbation is 7% of the base flow's kinetic energy, which is not a linear perturbation but the larger perturbation is used for visual clarity. (The effect of the perturbation on the base flow is qualitatively independent of the perturbation amplitude.) The two vortex pairs centred at $z/\lambda = 1.0$ and 2.0 in the base flow are squeezed toward $z/\lambda = 1.5$ by the two single vortices at $z/\lambda = 1.0$ and 2.0 in the eigenfunction. The two base vortices on either side of $z/\lambda = 1.5$ are weakened. This is seen more clearly when the percentage of the perturbation increases to 50% in figure 8 (*d*). If this character of the perturbation is maintained in the nonlinear state, we can expect that the two vortices on either side of $z/\lambda = 1.5$ in the base flow will disappear. Thus one out of every two pairs of vortices will be lost, i.e. merging of vortices occurs upon exiting the right-hand side of the Eckhaus boundary.

Our numerical results show that the number of vortices in the perturbation eigenfunction depends on b. Over a distance λ/b, there is one extra pair (left-hand side of the boundary) or one less pair (right-hand side of the boundary). For example when $\alpha = 2.3$ at $Re = 1.5Re_c$ (the right-hand side of Eckhaus boundary has $\alpha_{\text{right}} = 2.28$ at this Re), the maximum Eckhaus growth rate is given by $b = 0.1$. The corresponding eigenfunction shows that nine pairs of the perturbation vortices occupy the space of ten pairs of the base flow, i.e. only one pair will be lost for every ten pairs of base vortices. Thus when α is close to the Eckhaus boundary where the most unstable mode has small b, a relatively small number of vortices will be

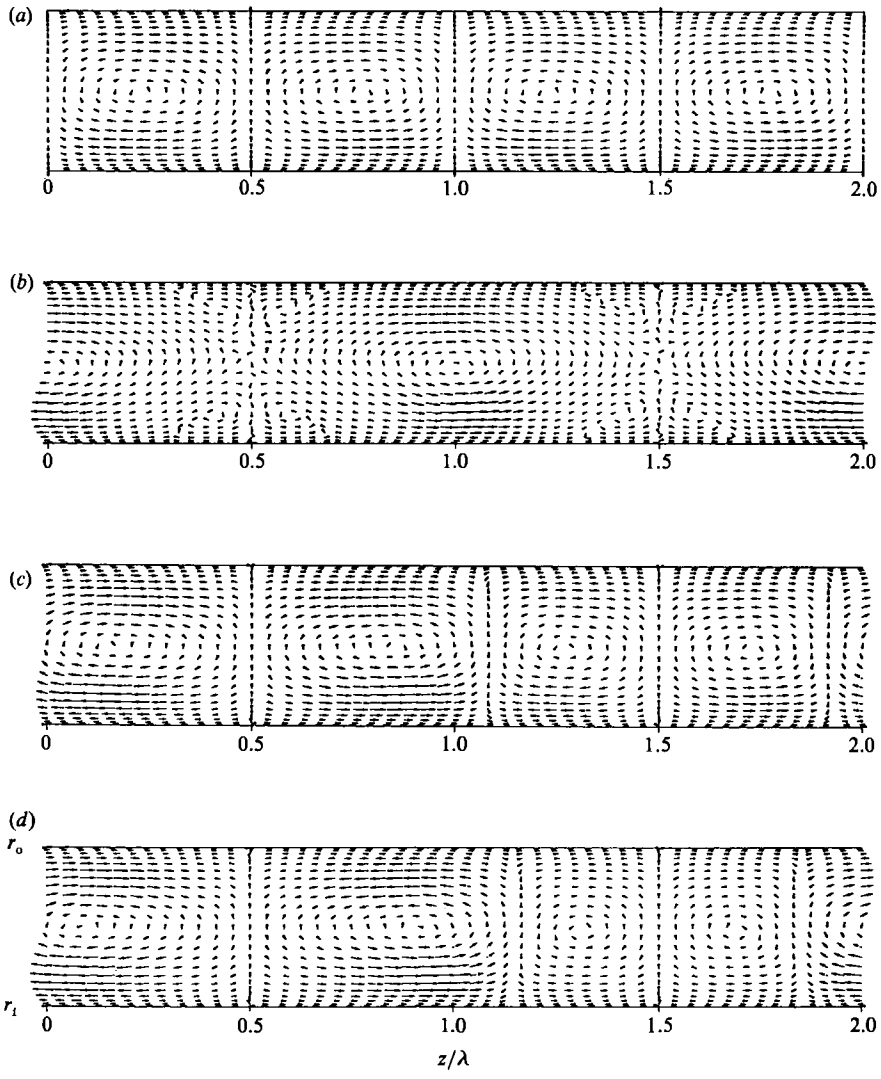

FIGURE 8. Same as figure 7 but at $\alpha = 2.475$, outside the right-hand side of the Eckhaus boundary ($\alpha_{\text{right}} = 2.425$). In (*c*), the kinetic energy of the most unstable model is 7% of the base flow's kinetic energy. In (*d*), the percentage of the most unstable mode is 50%.

produced or lost for a given number of base vortices. Further away from the boundary where the most unstable disturbance has $b = 0.5$, a larger number of vortices will be produced or lost.

In Taylor–Couette flow experiments, the spanwise wavenumber of the base vortex flow can be controlled by using adjustable spanwise walls (Dominguez-Lerma *et al.* 1986). Once Taylor vortices of the desired wavenumber are developed at high Re, the Eckhaus boundary can be found by decreasing Re until the flow loses its stability. Usually only one pair of vortices is produced or lost when the flow crosses the Eckhaus boundary. Based on our results, only a single pair appears or disappears because as the flow crosses the boundary into the unstable region, unstable perturbations occur with b slightly greater than zero. When unstable modes occur with b having a certain value, the finite span of the experimental device allows an

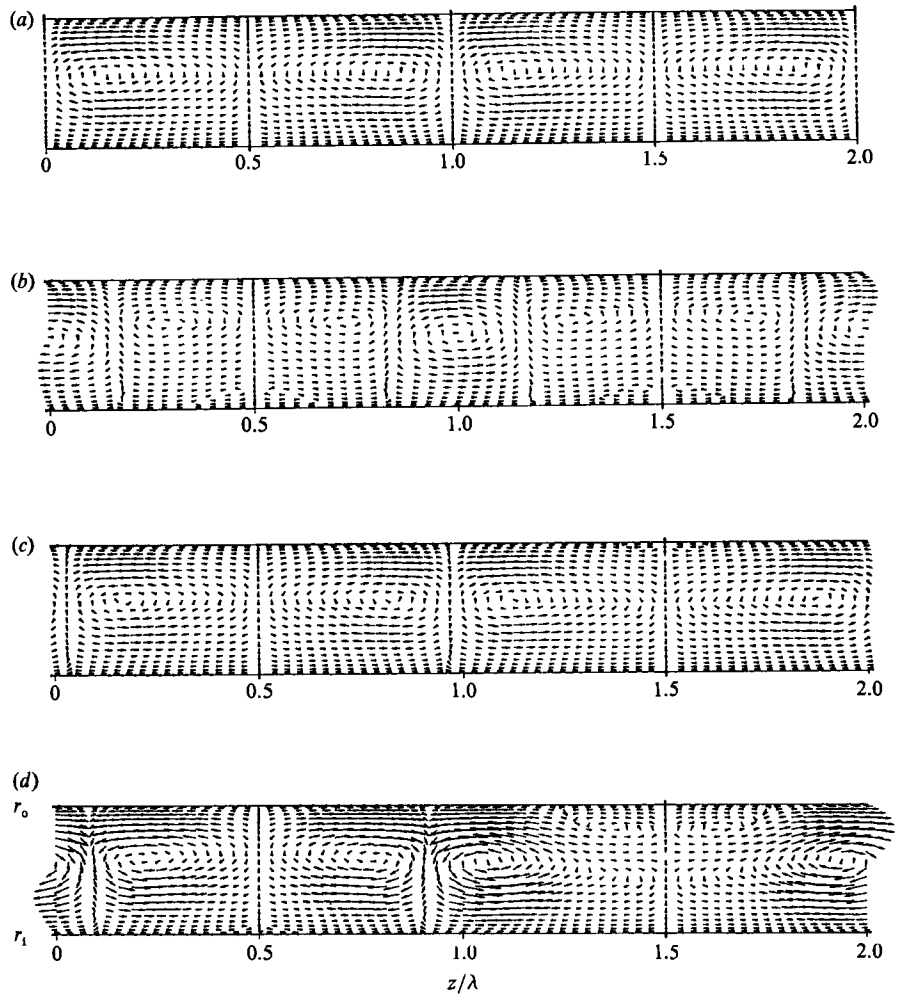

FIGURE 9. (*a*) Two-dimensional vortices, (*b*) their most unstable mode and (*c*, *d*) two-dimensional vortices + the most unstable mode, in a curved channel ($\eta = 0.975$) at $Re = 2.0Re_c$, $\alpha = 2.0$ projected onto the (r, z)-plane. In (*c*), the kinetic energy of the most unstable mode is 7% of the base flow's kinetic energy. In (*d*), the percentage of the most unstable mode is 20%. The most unstable mode has $b = 0.5$.

extra pair of vortices to be produced or absorbed: splitting or merging of vortex pairs occurs. The resulting vortex flow will then have a wavenumber which is inside the stable region.

The perturbation flow patterns from the Eckhaus instability seem to explain the Taylor–Couette experiment observations. However, one should be cautious when using the above results to explain the details of the splitting and merging processes because the actual effects of the perturbations on the base vortices could be highly nonlinear and dependent on finite span effects. For example, if certain pairs of vortices begin to split or merge earlier than others, the following readjustment of spanwise wavenumbers across the span will change the wavenumbers of other vortices and thus change the splitting or merging processes of these other vortex pairs. However, we can say that splitting always occurs outside the left-hand side of the boundary and merging outside the right-hand side.

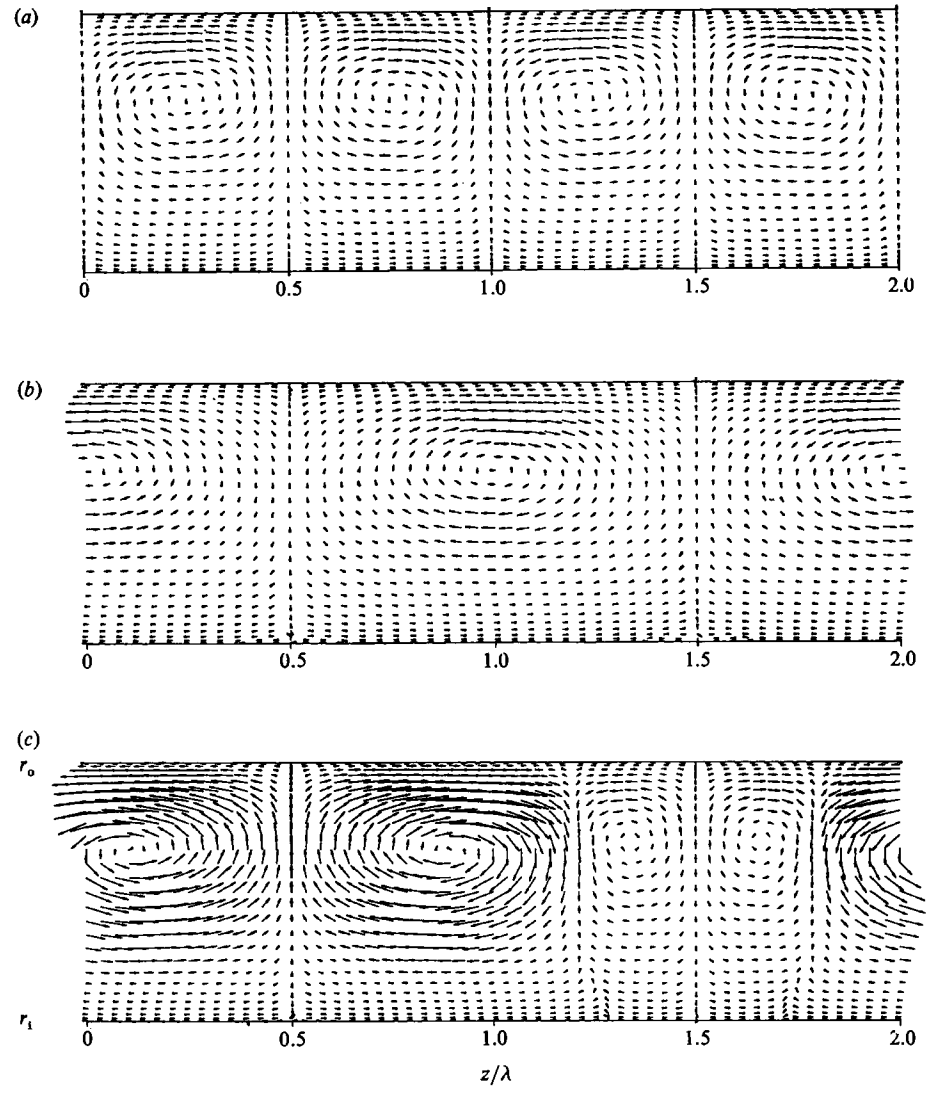

FIGURE 10. Same as in figure 9 but at $\alpha = 4.0$. In (*c*), the percentage of the most unstable mode is 50%.

4.2. *Channels with either curvature or rotation or both*

In channels with either curvature or rotation or both, most experiments have been done outside the Eckhaus stable region, where the maximum Eckhaus growth rate is positive and occurs at $b = 0.5$. Figures 9 and 10 show two vortex flows ($\alpha = 2.0$ in figure 9 and $\alpha = 4.0$ in figure 10), their most unstable modes and linear superpositions of base flows plus perturbations at $Re = 2.0Re_c$ in the curved channel with $\eta = 0.975$. Other unstable modes for different α (at $Re = 2.0Re_c$) can be found in figure 11 (the small waviness in figure 11*a*, *d* along $z/\lambda = 0.5$, 1.5 is caused by extremely small velocities being plotted with a fixed arrow size). At this Re, all spanwise wavenumbers of the base flow are unstable to Eckhaus instability. In all three figures, $z/\lambda = 0$, 1.0 and 2.0 are the centres of the base vortex pairs, where the fluid flows from the concave wall to convex wall (the inflow region). There are three types of unstable

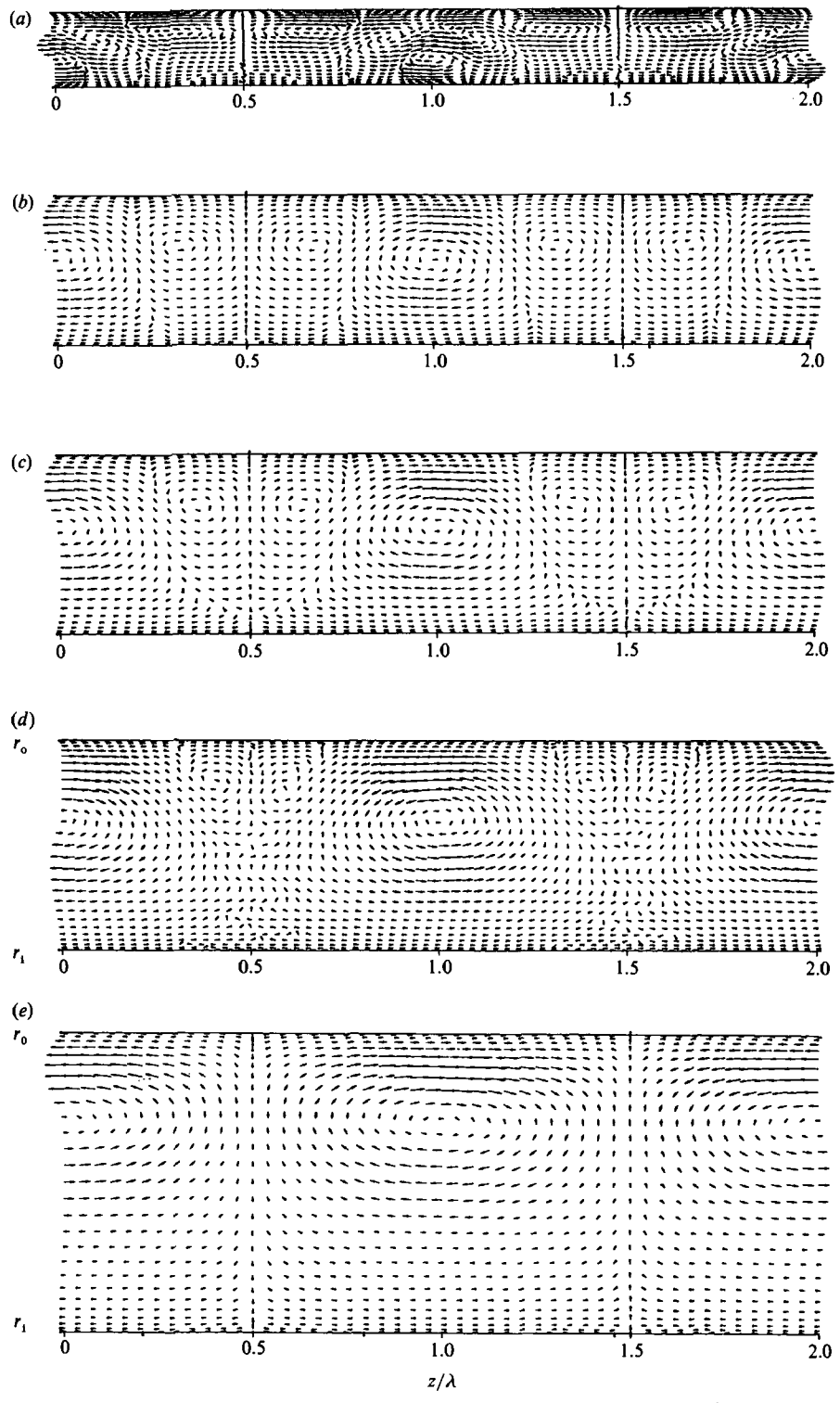

FIGURE 11. Most unstable modes (projected onto the (r, z)-plane) in a curved channel ($\eta = 0.975$) at $Re = 2.0Re_c$ and α: (*a*) $\alpha = 1.25$; (*b*) $\alpha = 2.5$; (*c*) $\alpha = 3.0$; (*d*) $\alpha = 3.5$; (*e*) $\alpha = 5.0$; $b = 0.5$ for all these modes.

modes shown in figures 9, 10 and 11 that occur for different ranges of α. In figure 11 (*a*), when $\alpha = 1.25$, there are five vortex pairs of the unstable mode in the space of two base pairs and the corresponding eigenvalue ($b = 0.5$) is complex. For $2.0 \leqslant \alpha \leqslant 3.5$ (figures 9*b*, 11*b–d*), three vortex pairs of the unstable mode take the space of two base pairs, though they do not have equal intensity or spanwise wavenumber. For α in this range, the eigenvalue with Eckhaus growth rate is always real for any b. In the range $\alpha > 3.5$ (figures 10*b* and figure 11*e*), there is only one vortex pair of the unstable mode in the space of two base pairs. In this range, Eckhaus eigenvalues are not always real for $b \neq 0.5$, but the eigenvalue with the maximum Eckhaus growth rate is still given by $b = 0.5$ and is real. Similar results are found in channels with rotation and curvature.

Heuristic arguments based on the flow patterns of the unstable modes in figures 9–11 suggest some vortices in the unstable modes will generate new vortex pairs, causing the splitting of base vortex pairs, and some will force base vortex pairs together, causing merging. For example, in figure 9 (*b*), a simple argument suggests it is more likely that the vortex pair at $z/\lambda = 1.5$ will develop than the one at $z/\lambda = 0.5$. This is because the large perturbation vortices centred at $z/\lambda = 1.0$ and $z/\lambda = 2.0$ induce flow at the centres of the base vortices on either side of $z/\lambda = 1.5$ causing them to spread apart. In contrast, near $z/\lambda = 0.5$ the large perturbation vortices induce motion at the centres of the base vortices straddling $z/\lambda = 0.5$ causing them to move together, obstructing the formation of the secondary vortex pair at $z/\lambda = 0.5$ (or $z/\lambda = 2.5$). Figure 9 (*c*) shows the base flow (figure 9*a*) superimposed with the unstable mode (figure 9*b*) whose kinetic energy has grown linearly to 7% of the base flow's kinetic energy. It can be seen that one new pair of secondary vortices begins to form at $z/\lambda = 1.5$ near the concave wall. The original vortex pairs centred at $z/\lambda = 1.0$ and 2.0 spread apart from $z/\lambda = 1.5$ and are squeezed toward $z/\lambda = 0.5$ and 2.5. As the energy level of the perturbation increases to 20% in figure 9 (*d*), the new vortex pair grows bigger and moves away from the concave wall. This is a splitting event, since a new vortex pair appears between the base vortex pairs centred at $z/\lambda = 1.0$ and 2.0. The two base vortex pairs centred at $z/\lambda = 1.0$ and 2.0 will be split apart by the new pair, yielding three pairs. Thus the vortex pair at $z/\lambda = 1.5$ in the most unstable eigenfunction is responsible for generating a new vortex pair in the outflow region of the base flow. When examining the eigenfunctions, the vortex pair which generates the new pair can be identified easily by the fact that it is centred about an inflow plane in the eigenfunctions.

As the wavenumber α of the base flow increases, the intensity of the pair responsible for splitting becomes weaker, as is shown in figure 11 (*b–d*). When $\alpha > 3.5$, this pair is absent, as shown in figures 10 (*b*) and 11 (*e*), and splitting cannot happen. In addition, as α increases, the single vortices centred at $z/\lambda = 0$, 1.0 and 2.0 in the most unstable eigenfunction become stronger. These vortices are responsible for merging two base pairs together, as is seen in figure 10 at $\alpha = 4.0$. Figure 10 (*c*) shows the base flow (figure 10*a*) perturbed by 50% (kinetic energy) of the most unstable mode (figure 10*b*). Two neighbouring vortices (centred at $z/\lambda = 1.5$) of the two base vortex pairs become smaller and weaker while the other two become bigger and stronger. As the amplitude of the perturbation is increased further, the two vortices on either side of $z/\lambda = 1.5$ eventually disappear while the other two vortices form into one pair. Thus two pairs merge into one pair. The large perturbation amplitudes used to produce figures 9 (*d*) and 10 (*c*) are not linear amplitudes, but are used for visual clarity. The qualitative effects of the perturbations are independent of their amplitude.

The most unstable modes thus have two different effects on the base vortex flow, associated either with splitting or merging. There is not a clear cut wavenumber α that divides the effects of the most unstable modes into vortex splitting or merging regions. For example at $\alpha = 3.0$ in figure 11(*c*), the small vortex pair at $z/\lambda = 0.5$ tends to cause the appearance of a new pair in the base flow at $z/\lambda = 0.5$, while the single vortices at $z/\lambda = 0$, 1.0 and 2.0 tend to cause merging of the two vortex pairs in the base flow on either side of $z/\lambda = 1.5$ and this merging effect in return allows room for the appearance of the new pair. Thus when this eigenfunction is imposed on the base flow, splitting and merging of vortex pairs are seen to occur at the same time, but at spanwise locations separated by one wavelength. For general α and b, we find no strict relation between b and the number of vortices in the most unstable modes. It depends on both b and α. However, it is always true that base vortex pairs with large wavenumbers merge, whereas small wavenumbers split. Since base vortices with $\alpha < 1.5$ are not likely to occur experimentally because of the low growth rate of the primary instability at this α, subharmonic splitting and merging mechanisms will be the dominant feature of splitting and merging of vortex pairs in channels with either curvature or rotation or both. Since all two-dimensional vortices are unstable to spanwise perturbations at high enough Re, the splitting and merging of vortex pairs, as suggested by figures 9–11, will continually occur.

Support for our results can be found from existing flow visualizations in channels with either curvature or rotation or both given by various authors (Ligrani *et al.* 1990; Ligrani & Niver 1988; Alfredsson & Persson 1989; Matsson & Alfredsson 1990) as well as in nonlinear simulations (§7). Splitting and merging of vortex pairs is prevalent in these experiments. When visualized with reflective flakes, in plan view the splitting of vortex pairs is indicated by two new bright streaks which represents a vortex pair first appearing between two existing streaks. The existing streaks are then split (spread) apart by the two new streaks. This is seen for example in figure 6(*d*), (*f*) of Alfredsson & Persson (1989) in channels with rotation or in figure 14(*d*) of Matsson & Alfredsson (1990) in a channel with both curvature and rotation. The disappearance of vortex pairs is indicated by adjacent bright streaks which occasionally merge together (cf. figure 6*e* of Alfredsson & Persson 1989; figure 14*d* of Matsson & Alfredsson 1990). We suggest that subharmonic splitting and merging are the mechanisms behind these phenomena. Splitting and merging of vortex pairs can also be found in flat plate boundary layers with rotation (Masuda & Matsubara 1989) and concave wall boundary layer (Bippes 1978) experiments. A similar Eckhaus instability mechanism in these flows may cause the splitting and merging of vortex pairs.

The actual splitting and merging processes observed in experiments are complicated and nonlinear. Ligrani *et al.* (1990) and Ligrani & Niver (1988) provide observations of these processes in a curved channel ($\eta = 0.979$). During the splitting of vortex pairs, according to their observation, new vortex pairs are formed first near the concave wall between other pairs, then followed by a readjustment of spanwise wavenumber. When viewed in the radial-spanwise plane, the new vortex pairs appear to 'pop' out of the concave wall. Ligrani & Niver called them secondary vortices. This observation is consistent with our result in figure 9(*c*, *d*). The formation of the secondary vortices observed by Ligrani & Niver (1988) may thus be due to Eckhaus instability.

Further numerical results show that base vortices which have secondary vortices between them are much more unstable to spanwise perturbations. For certain α we find two base solutions exist, one with secondary vortices and one without. Such non-

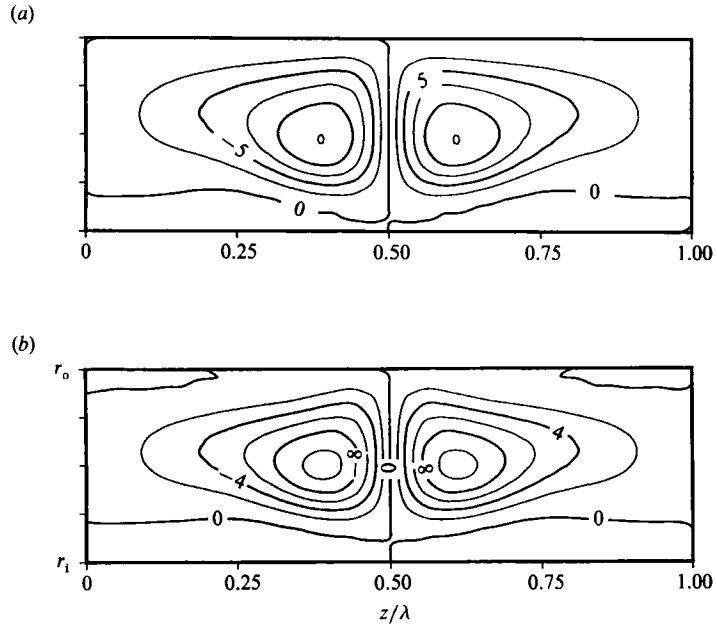

FIGURE 12. Streamfunctions of two-dimensional vortices in a rotating channel ($Ro = 0.03$) at $Re = 472.5$, $\alpha = 2.0$: (a) without secondary vortices; (b) with secondary vortices. The Eckhaus growth rates are (a) $\sigma = 0.059$ and (b) $\sigma = 0.108$.

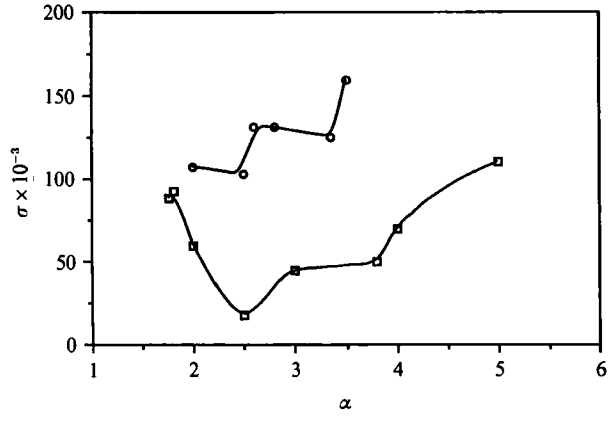

FIGURE 13. Comparison of the maximum Eckhaus growth rate σ of two-dimensional vortices ○, with secondary vortices and □, without secondary vortices at $Re = 472.5$ in a rotating channel ($Ro = 0.03$) for $1.75 \leqslant \alpha \leqslant 5.0$; $b = 0.5$ yields the maximum Eckhaus growth rate for each α.

uniqueness also occurs in Taylor–Couette flow (e.g. Mayer-Spasche & Keller 1985). Figure 12 shows the stream functions of the flows without and with such secondary vortices in a channel with rotation ($Ro = 0.03$, $Re = 472.5$). The related Eckhaus growth rate jumps from 0.059 in the absence of the secondary vortices to 0.108 when the secondary vortices are present. Comparison for other α can be found in figure 13 where there is always a large increase in the Eckhaus growth rate when secondary vortices are present.

The above arguments are based on linear theory, which only applies to the beginning of splitting and merging processes prior to the onset of nonlinearity. In experiments, spanwise periodicity is not imposed so that if any two vortex pairs start

to merge with each other earlier or more rapidly than others, neighbouring vortex pairs will move in, causing a decrease in spanwise wavenumber of these neighbouring vortices (readjustment of α), and suppression of their merging. Similarly, if certain vortex pairs begin to split apart earlier or more rapidly than others, they will tend to squeeze neighbouring vortices and obstruct the splitting of these neighbouring vortex pairs. Thus it is not surprising that in experiments the splitting and merging processes produce many patterns once the base vortices begin to lose their symmetry and move toward or away from each other. However, two to three splitting and two to one merging mechanisms are likely to be one of the major features of the transition from vortex flow to turbulence in channels with either curvature or rotation or both.

5. Wavenumber selection

Our discussion in §4 suggests that the splitting and merging processes are sensitive to the rate at which local perturbations develop, i.e. to the local Eckhaus growth rate σ. Vortices which yield smaller σ produce a region where the perturbations take a longer time to develop, so that splitting or merging processes occurring elsewhere will suppress the splitting or merging of vortex pairs with low Eckhaus growth rate. Thus vortices with relatively lower growth rate are more likely to be observed in experiments. Figure 14 shows a plot of the Eckhaus growth rate $\sigma(b = 0.5)$ *vs.* α at different Re in the curved channel with $\eta = 0.975$. For $Re \geqslant 2.2Re_c$, $\sigma(\alpha)$ has a minimum. When contours of σ are plotted in a (α, Re)-plane this minimum appears as a valley and we call it the Eckhaus valley. As Re increases, both sides of the valley become steeper. Based on our above discussion, observed wavenumbers should be close to this valley. For $Re < 2.2Re_c$, σ varies little with α and here Eckhaus instability does not play a major role in the wavenumber selection process. Thus when $Re < 2.2Re_c$, without any other nonlinear selection mechanism the observed wavenumbers should be close to the ones with maximum primary growth rate, since these vortices develop most rapidly from the one-dimensional Poiseuille type flow. Figure 15 shows the Eckhaus valley for $\eta = 0.975$ in comparison with the wavenumbers observed by Kelleher, Flentie & McKee (1980) in a curved channel with $\eta = 0.979$. Also shown are the wavenumbers with maximum primary growth rate and maximum pressure gradient (Finlay *et al.* 1988). For $Re < 2.2Re_c$, the observed wavenumbers are close to the ones with maximum primary growth rate. For $Re \geqslant 2.2Re_c$, the observed wavenumbers are close to the Eckhaus valley. This is consistent with our discussion.

A similar comparison can be found in figure 16 at $Re = 175$ and 472.5 in channels with rotation. The wavenumbers were measured by Alfredsson & Persson (1989) at three different downstream locations $y/d = 40$, 80 and 120. In figure 16(*a*) the observed wavenumbers at $y/d = 40$ are closer to those with maximum primary growth rate than the Eckhaus valley. As the downstream distance increases to 80 and 120, the observed wavenumbers become much closer to the Eckhaus valley. This suggests that near the entrance of the channel where the flow is still developing from one-dimensional Poiseuille type flow to two-dimensional vortices, the primary instability plays an important role in the wavenumber selection process. Once the two-dimensional vortices are more fully developed, the Eckhaus instability sets in and the wavenumbers of the vortices are selected by the Eckhaus valley. This is particularly noticeable for $Ro \geqslant 0.05$ ($Re/Re_c \geqslant 2.566$) in figure 16(*a*), where the Eckhaus valley and observed wavenumbers diverge significantly from the curve of maximum primary growth rate.

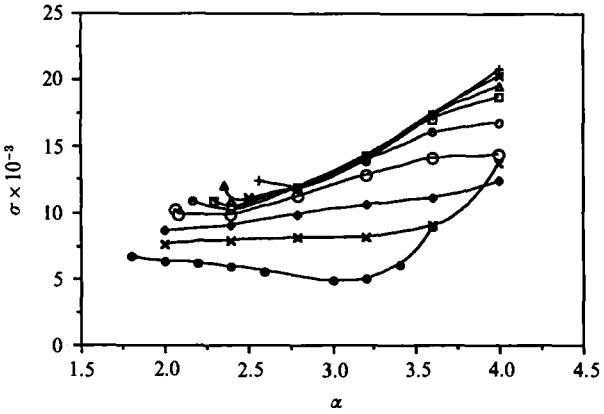

FIGURE 14. Maximum Eckhaus growth rate σ as a function of the spanwise wavenumber α of two-dimensional vortices in a curved channel ($\eta = 0.975$) at Re: ●, $Re = 1.5Re_c$; ×, $Re = 1.7Re_c$; ◇, $Re = 1.9Re_c$; ○, $Re = 2.2Re_c$; ○, $Re = 2.5Re_c$; □, $Re = 2.8Re_c$; △, $Re = 3.0Re_c$; ★, $Re = 3.25Re_c$; +, $Re = 3.5Re_c$.

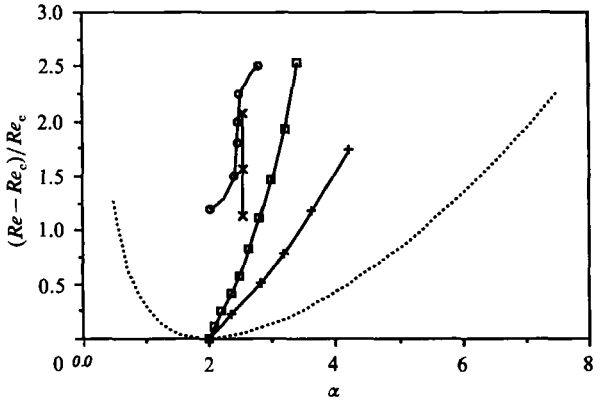

FIGURE 15. ○, Eckhaus valley; □, the curves of maximum primary growth rate; and +, maximum pressure gradient of Finlay *et al.* (1988) in a curved channel with $\eta = 0.975$, and ×, the wavenumbers of two-dimensional vortices observed by Kelleher *et al.* (1980) in $\eta = 0.979$. -----, The primary stability of Finlay *et al.* is included for reference.

In channels with rotation $Ro < 0.25$, the critical Reynolds number Re_c decreases as the rotation number Ro increases (Alfredsson & Persson 1989). So for a given Re, Re/Re_c increases as Ro increases. Our results indicate the Eckhaus valley becomes deeper and narrower with increasing Re/Re_c, making it a more effective wavenumber selection mechanism at higher Re/Re_c. Figure 16(*a*) indeed shows that the effect of the Eckhaus instability on wavenumber selection becomes more obvious as Re/Re_c increases. Figure 16(*b*) shows that at high Re/Re_c ($3.37 < Re/Re_c < 6.3$ in figure 16*b*) the Eckhaus valley provides a much better prediction for the observed wavenumber than the primary instability.

Similar results are found in channels with both curvature and rotation. Figure 17 shows a plot of the maximum Eckhaus growth rate *vs.* α at different Ro in the curved channel with $\eta = 0.975$ and $Re = 180$. As $|Ro|$ increases in figure 17, the slopes of the Eckhaus valley become steeper. Increasing $|Ro|$ is thus similar to increasing Re in curved channels in that both cause an increase in the slope of the side of the Eckhaus valley. Figure 18 shows the corresponding Eckhaus valley and the wavenumbers

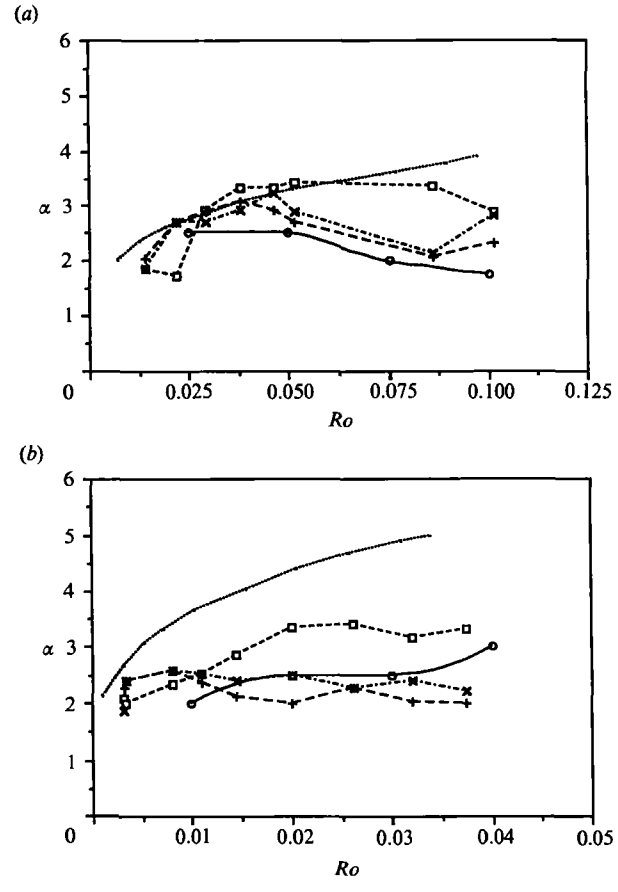

FIGURE 16. ○, Eckhaus valley, -----, the curve of maximum primary growth rate and the observed wavenumbers of two-dimensional vortices of Alfredsson & Persson (1989) in a rotating channel at different downstream locations y/d: □, $y/d = 40$; ×, $y/d = 80$; +, $y/d = 120$. In (*a*), $Re = 175$; in (*b*), Re = 472.5.

which have the maximum primary growth rate. Matsson & Alfredsson (1990) provide experimental flow visualizations of vortices in channels with both curvature and rotation but the wavenumbers of the vortices are not available in their publication, so no comparison is made here.

Matsson & Alfredsson (1990) observe a range of Ro where rotation opposes curvature and restabilizes the flow to a one-dimensional state. When $Ro = 0$ at $Re = 180$, they observe two-dimensional vortices. When Ro decreases to -0.015, they observe a complete cancellation of vortices by rotation. In our numerical computation, we cannot obtain any steady two-dimensional vortices near this parameter range. As Ro decreases further, two-dimensional vortices begin to develop again in line with Matsson & Alfredsson's results.

At sufficiently high Re/Re_c and at locations far enough downstream from the inlet, two-dimensional vortices in curved and/or rotating channels lose their stability to streamwise perturbations and develop into three-dimensional wavy vortices (Finlay *et al.* 1988; Finlay 1990). The spanwise wavenumber selection process is then no longer just determined by the Eckhaus instability. For example, in the curved channel with $\eta = 0.975$, two-dimensional vortices first lose their stability to

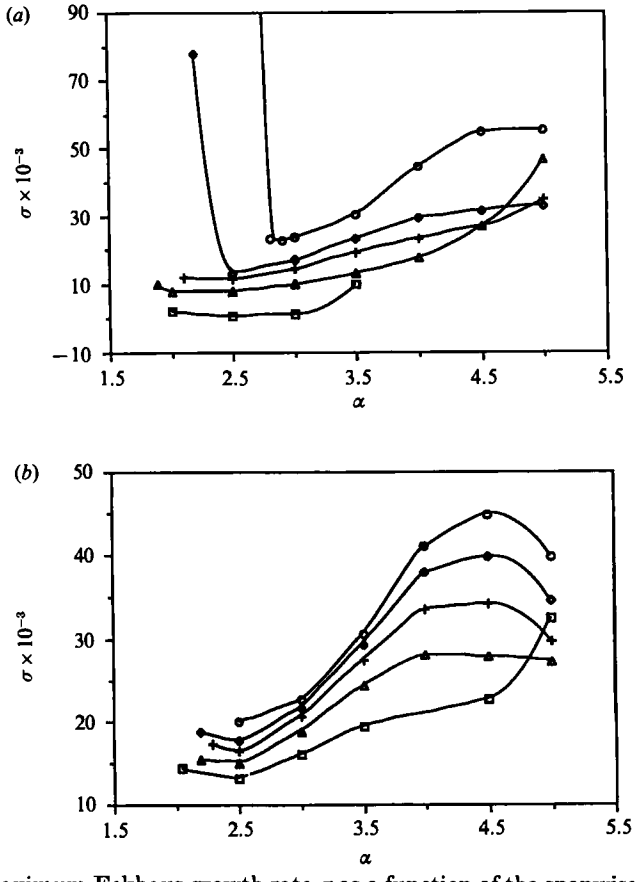

FIGURE 17. Maximum Eckhaus growth rate σ as a function of the spanwise wavenumber α of two-dimensional vortices in a curved-rotating channel ($\eta = 0.975$) at $Re = 180$. In (a), $Ro < 0$: □, $Ro = -0.025$; △, $Ro = -0.035$; +, $Ro = -0.045$; ◇, $Ro = -0.055$; ○, $Ro = -0.11$. In (b), $Ro > 0$: □, $Ro = 0.015$; △, $Ro = 0.025$; +, $Ro = 0.035$; ◇, $Ro = 0.045$; ○, $Ro = 0.055$.

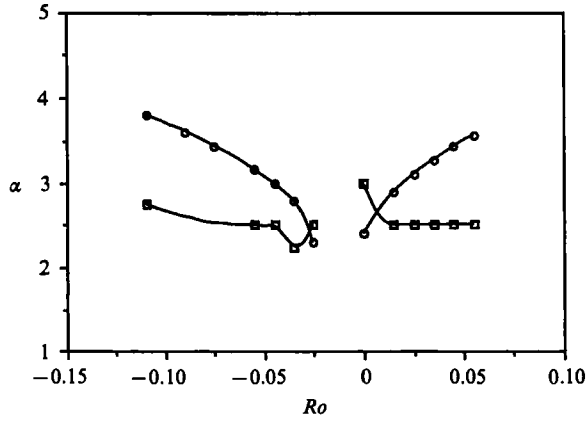

FIGURE 18. □, Eckhaus valley and ○, the curve of maximum primary growth rate for a curved-rotating channel ($\eta = 0.975$) at $Re = 180$.

streamwise perturbations at $Re'_c = 1.2Re_c$ and $\alpha'_c = 2.2$, developing into undulating wavy vortices (Finlay *et al.* 1988) and calculations by us show at $Re''_c = 1.92Re_c$ and $\alpha''_c = 2.58$, they develop into twisting vortices (other values of α require larger Re for wavy vortices to develop). Little is known about the stability of three-dimensional vortices in channels with either curvature or rotation or both. The effect of the wavy instability on wavenumber selection is unknown. In their numerical simulations, Finlay *et al.* (1988) reported that streamwise waviness delayed the onset of vortex doubling to higher Re.

Competition between Eckhaus instability and wavy instability will be dominated by wavy instability when the corresponding growth rates of Eckhaus instability are much less than those of the wavy instability. For example, in figure 16(*a*), the ratio of the average Eckhaus growth rate to the wavy growth rate is about 0.7. Here good agreement is found between the observed wavenumbers and the Eckhaus valley. Thus, when the Eckhaus growth rate is not that much less than that of the wavy instability, it appears that splitting and merging occur before the vortices develop into three-dimensional vortices and the Eckhaus instability plays an important role in wavenumber selection. In figure 16(*b*) this ratio is 0.2, much smaller than in figure 16(*a*). The difference between the Eckhaus valley and the observed wavenumbers suggests that there is some effect due to the three-dimensionality of the vortices. However, little can be said on this issue without performing a stability analysis of three-dimensional wavy vortex flow.

6. Recurrent splitting and merging

The repetitive appearance of splitting and merging was first reported by Ligrani & Niver (1988) in a curved channel ($\eta = 0.979$). It only occurred at certain Re ($Re = 2.03Re_c$ and $2.14Re_c$). The flow visualization results obtained by Alfredsson & Persson (1989) in channels with rotation (cf. their figure 6*e*) and by Matsson & Alfredsson (1990) in channels with both curvature and rotation (cf. their figure 14*d*) suggest that such a phenomenon also exists in rotating or curved-rotating channels. For example in a curved-rotating channel at $Re = 180$, $\eta = 0.975$, $Ro = -0.025$ (figure 14*d* of Matsson & Alfredsson 1990), we can see that a short time after two vortex pairs split apart into three pairs, two of these three pairs merge back into one and then split again with the other one into three pairs. The mechanism behind this is still the subharmonic two to one merging and two to three splitting. Our discussion in §4 indicates that when the flows resulting from splitting or merging have the same Eckhaus growth rate as before the split or merge, the repetitive appearance of splitting and merging will occur. This may happen in two cases: (i) where the Eckhaus valley is very flat and (ii) when the wavenumbers of the flows resulting from splitting and merging alternate between opposite sides of the Eckhaus valley where the Eckhaus growth rates are nearly the same. It is difficult to predict when the second case will happen. Compared with the first case, the conditions required for the second case are much more restrictive, so the chance of it being observed is considerably less than in case (i). In the first case, the Eckhaus growth rate is approximately the same for any vortex pair, so no vortex wavenumber is significantly more stable than any other. There is thus a good chance for the recurrent appearance of splitting and merging. In the curved channel with $\eta = 0.975$, this range is $1.7 \leqslant Re/Re_c \leqslant 1.9$ (figure 14). Ligrani & Niver observed repetitive splitting and merging when close to this region. For Matsson & Alfredsson's case, the corresponding Eckhaus growth rate is shown in figure 17(*a*). In the range $-0.025 \leqslant Ro \leqslant -0.035$,

the Eckhaus growth rate curve is relatively flat near its minimum value. Repetitive splitting and merging thus mostly appears to occur in parameter regimes where the Eckhaus valley is relatively flat.

7. Nonlinear simulation of splitting and merging of vortex pairs

The results on splitting and merging given in §4, 5 and 6 are based on linear stability theory. Nonlinearity sets in once a splitting or merging event develops past the initial linear stage. In order to study the nonlinear aspect of the problem and how it affects the validity of our linear theory results, we use the Galerkin spectral numerical method of Moser, Moin & Leonard (1983) to simulate the axisymmetric, time-dependent, incompressible Navier–Stokes equations in a curved channel. The code is a modification of the one used to study wavy Taylor vortices by Moser *et al.* (1983), wavy Dean vortices by Finlay *et al.* (1988), wavy vortices in rotating channel flow by Finlay (1990) and to perform a direct simulation of turbulence in the curved channel (Moser & Moin 1984, 1987). Periodic boundary conditions are used in the spanwise direction. We will discuss two simulations. The first of these demonstrates the nonlinear details of splitting and merging, while the second demonstrates wavelength selection due to Eckhaus instability.

According to the linear stability analysis of §4, the spanwise wavenumber of the most unstable disturbance is $\frac{1}{2}\alpha$ (i.e. $b = 0.5$), where α is the spanwise wavenumber of base flow. In our first simulation, the spanwise computational domain is chosen initially to include two complete vortex pairs. Small, two-dimensional random disturbances ($< 0.1\%\bar{U}$) are used to perturb the initial two-dimensional vortex flow. The solution progresses in time with constant mass flux imposed. The energies in the highest modes are monitored to ensure that adequate resolution is achieved. The simulation parameters are $Re = 1.776Re_c$ and $\eta = 0.975$. The wavenumber of the initial vortices is $\alpha = 2.0$. At these parameters, we use 40 spanwise Fourier modes and 32 Chebyshev polynomials in the radial direction.

Figure 19 shows the flow velocity projected onto the (r, z)-plane at different timesteps. The initial conditions for the simulation are shown in figure 19(*a*). The centres of the initial two pairs are at $z/\lambda = 0.5$ and 1.5. At $t = 5700d/2\bar{U}$ in figure 19(*b*), a small new vortex pair has begun to form near $z/\lambda = 0$ (and $z/\lambda = 2.0$). The original pairs are squeezed toward $z/\lambda = 1.0$. During the early stage of the simulation when the disturbances are very small, the temporal growth rate of the disturbances is $0.0079 + 0.0\mathrm{i}$, compared to $0.0080 + 0.0\mathrm{i}$ for the most unstable mode from linear stability analysis. This shows that the most unstable eigenfunction from the linear theory is indeed the dominant unstable disturbance (and also further verifies our linear stability code). The appearance of the new pair of vortices in figure 19(*b*) is associated with a splitting event and is caused by the growth of the most unstable eigenfunction from the random initial disturbances. The flow patterns obtained in the nonlinear simulation up to this time are very similar to those obtained from the linear stability analysis by imposing the most unstable eigenfunction on the base flow, as depicted in figure 9(*c*, *d*). When $t = 6200d/2\bar{U}$ (figure 19*c*), the new pair is well developed and the computational box is filled with three strong pairs. At the same time, a merging process of the two original pairs has begun. This can be seen more clearly in figure 19(*d*). The merging process is similar to that depicted by linear stability analysis in figure 10(*c*): two neighbouring vortices of the two original vortex pairs become weaker while the other two vortices become stronger. By the time $t = 8450\mathrm{d}/2U$ in figure 19(*e*), two vortices have completely disappeared and the two

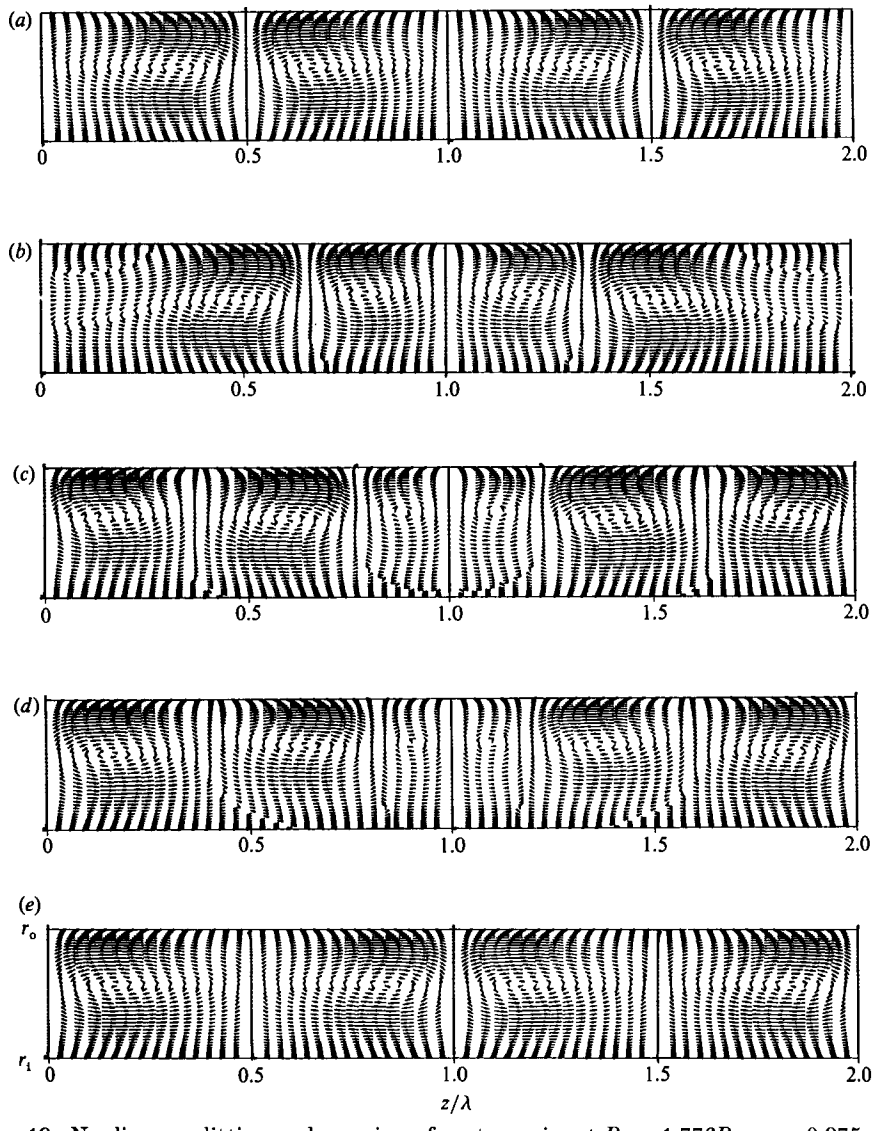

FIGURE 19. Nonlinear splitting and merging of vortex pairs at $Re = 1.776Re_c$, $\eta = 0.975$. The flow is projected onto the (r, z)-plane at time (*a*) 0, (*b*) $5700d/2\bar{U}$, (*c*) $6200d/2\bar{U}$, (*d*) $6450d/2\bar{U}$ and (*e*) $8450d/2\bar{U}$. The vortices in (*a*) and (*e*) have $\alpha = 2.0$.

original vortex pairs have merged into one pair. The new pair of vortices that appeared owing to splitting has adjusted itself so that the velocity field of the flow has returned exactly to its original pattern, but with a spanwise shift of half a wavelength. The above splitting and merging processes continue periodically in time. Compared with the predictions from linear theory in figures 9 and 10, the similarity is striking. The simultaneous splitting and merging effects of the most unstable eigenfunction discussed in §4 are demonstrated clearly in figure 19. When splitting occurs, a new pair is always generated between two base pairs. When merging occurs, two base pairs merge into one pair.

Outside the Eckhaus stable region, all wavenumbers are unstable. However, our discussions in §5 indicate that vortices with wavenumbers in the Eckhaus valley are

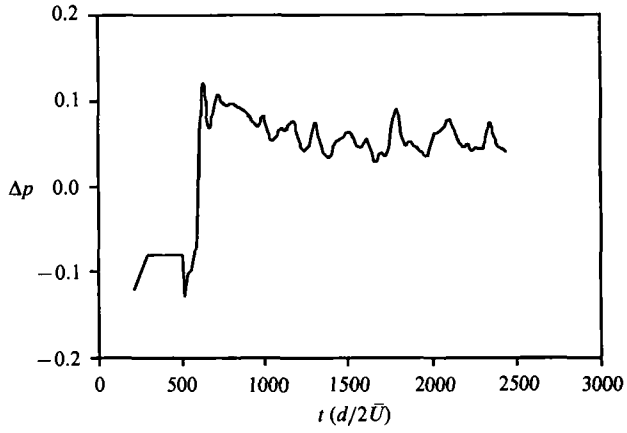

FIGURE 20. The pressure gradient parameter Δp as a function of time at $Re = 2.2Re_c$ in a curved channel $\eta = 0.975$ with aspect ratio $\Gamma = 6\pi{:}1$ and periodic spanwise boundary conditions.

the least unstable to splitting and merging and are likely to be observed more often in experiments. In order to study the validity of this result in the presence of nonlinear splitting and merging processes and the interactions between vortices with different wavenumbers, we select the aspect ratio of our computational box in our second simulation to be $6\pi{:}1$. Periodic boundary conditions are again imposed in the spanwise direction, but now over a spanwise extent three times larger than in the first simulation. Since an integer number of pairs of vortices must appear in the simulation region, the average wavenumber of the vortices is restricted to $\frac{1}{3}n$, where n is an integer. We use 96 spanwise Fourier modes and 16 Chebyshev polynomials (in the radial direction) in this simulation.

We start the simulation using curved channel Poiseuille flow with low-amplitude random noise ($< 0.1\%\bar{U}$) superimposed and use $Re = 2.2Re_c$ in a curved channel having $\eta = 0.975$. Figure 20 shows the time development of the pressure gradient parameter Δp, defined as (Finlay *et al.* 1988)

$$\Delta p \equiv \frac{(\overline{\partial P}/\partial\theta) - (\partial P/\partial\theta)}{(\partial P/\partial\theta)}, \tag{7.1}$$

where $-(1/r)(\partial P/\partial\theta)$ is the streamwise pressure gradient of curved channel Poiseuille flow and $-(1/r)(\overline{\partial P}/\partial\theta)$ is the streamwise pressure gradient of the vortex flow averaged over the computational box.

After $t = 500d/2\bar{U}$, finite-amplitude two-dimensional vortices develop rapidly. In figure 20, the corresponding Δp increases dramatically. Figure 21 (*a*) shows contours of the Stokes stream function at $t = 650d/2\bar{U}$. Excluding the three pairs near the centre of the box where a splitting event is underway, the average wavenumber of the vortices at this time is 2.79. This is very close to the wavenumber $\alpha = 2.82$ which has the maximum primary instability growth rate (see figure 15). This demonstrates that during the early stage of the development of vortex flow, the primary instability does play an important role in wavenumber selection process, as suggested in §5.

As the solution proceeds in time, the flow goes through a sequence of splitting and merging processes and there is a decrease in the average wavenumber of the vortices until $t = 1300d/2\bar{U}$. For $t > 1300d/2\bar{U}$, the wavenumber of the vortices remains near the Eckhaus valley, which is rather flat and lies between $\alpha = 2.1$ and $\alpha = 2.35$ (see figure 14). But it continues to fluctuate owing to splitting and merging events. The

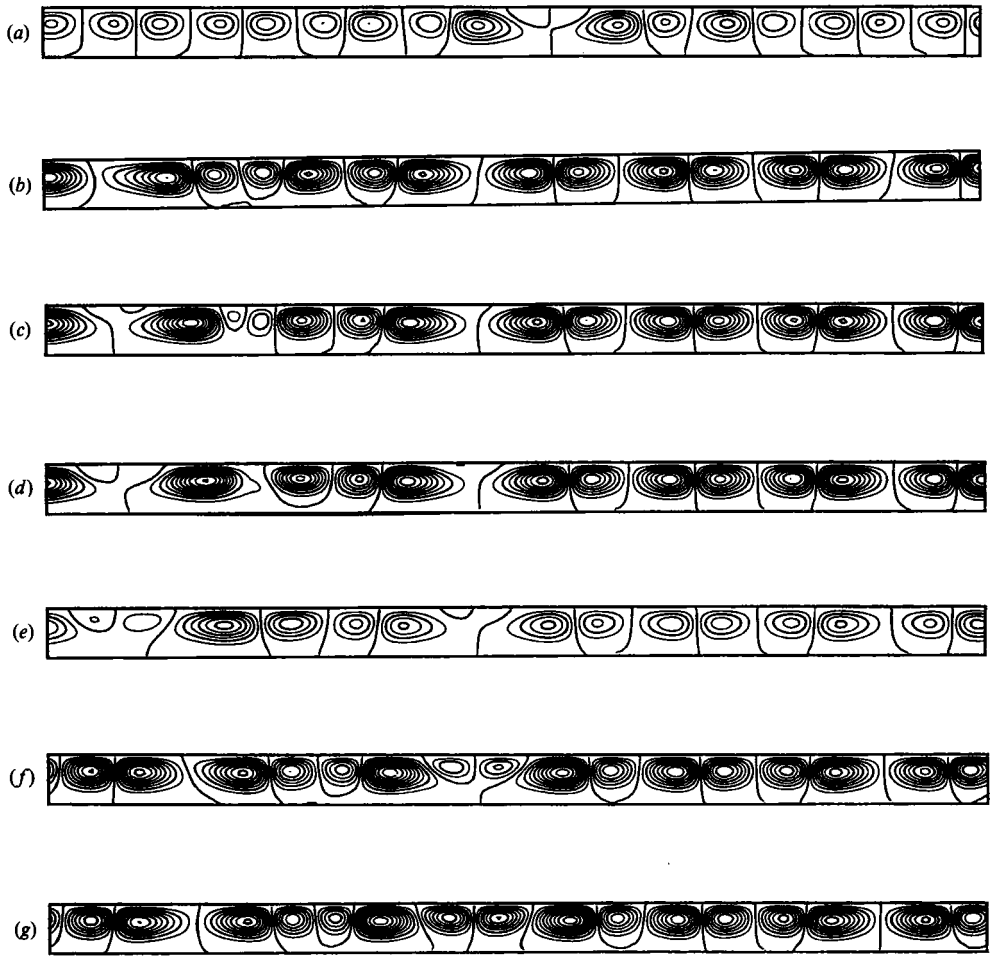

FIGURE 21. Contours of Stokes stream function for curved channel flow at $Re = 2.2Re_c$, $\eta = 0.975$ are shown in the (r, z)-plane at time (*a*) $650d/2\bar{U}$, (*b*) $1850d/2\bar{U}$, (*c*) $1949d/2\bar{U}$, (*d*) $1978d/2\bar{U}$, (*e*) $2009d/2\bar{U}$, (*f*) $2069d/2\bar{U}$ and (*g*) $2099d/2\bar{U}$. The aspect ratio is $\Gamma = 6\pi : 1$, with periodic spanwise boundary conditions.

time record of Δp is useful for determining when splitting and merging events occur, since according to Finlay *et al.* (1988), for $\alpha < 3.7$ at $Re = 2.2Re_c$ and $\eta = 0.975$, the smaller α is, the smaller Δp is. Examining $\Delta p(t)$ and the velocity field, we find that whenever Δp decreases, merging processes are underway, but whenever ΔP increases, there are splitting processes dominating the flow. Figure 21 (*b–g*) show a typical cycle of the flow development from $t = 1850d/2\bar{U}$ to $2099d/2\bar{U}$. In figure 21 (*b*), the average wavenumber of the first three vortex pairs from the left-hand side of the box is 2.37, while the rest of the vortices have a wavenumber of 2.19, which is in the Eckhaus valley. There is a merging process just underway between the first two pairs from the left. This merging process becomes clearer in figure 21 (*c*). For the rest of the vortices, there is a very small decrease in wavenumber from 2.19 to 2.13. When $T = 1978d/2\bar{U}$ in figure 21 (*d*), one vortex pair has completely disappeared. The pressure gradient Δp reaches a local minimum (cf. figure 20).

In figure 21 (*c*), there is a new pair beginning to appear near the left-hand end of the box. This becomes clearer in figure 21 (*d*) and 21 (*e*). Another new pair also begins

to develop near the centre of the box where the vortices have smaller α. The rest of the vortices remain essentially unchanged. When $t = 2069d/2\bar{U}$ in figure 21 (f), the new pair near the left-hand side is almost fully developed. The other one near the centre continues to grow. The rest of the vortices have been squeezed somewhat and there is an increase in their wavenumbers (from 2.17 in figure 21 d to 2.57 in figure 21 f). It can be seen that the second and third pairs from the left in figure 21 (f) have begun a merging process. In figure 21 (g), the new pair near the centre has completed its development. At this time, the wavenumber is nearly the same for all vortices and the average wavenumber is 2.67. This high wavenumber causes a local maximum in Δp. The merging of the second and third pairs from the left proceeds. As these two pairs continue to merge, the other vortices experience an adjustment in their wavenumbers which results in smaller wavenumbers. From figure 21 and similar results at other times in the simulation, we find that when the wavenumber of several pairs of neighbouring vortices is close to the Eckhaus valley, the wavenumber of these pairs remains nearly constant for a long time and their adjustment due to splitting and merging events is very weak, as is the case in figure 21 (b–d). However, when the wavenumber of two or more neighbouring pairs is not close to the Eckhaus valley, there is a rapid and large change in wavenumber.

The simulation results also show that when the average wavenumber of the vortices is near the Eckhaus valley, the development of splitting and merging is relatively slow. When the wavenumbers of vortices are far from the Eckhaus valley, the pressure gradient experiences rapid and large fluctuations as a result of simultaneous multiple splitting or merging processes. A vortex flow with wavenumbers far from the Eckhaus valley does not last long. Thus, when averaged on time, the average wavenumber is close to the Eckhaus valley.

Figure 21 also demonstrates repetitive splitting and merging. In figure 21 (b–g), the first two pairs from the left merge, and then this is followed by a splitting event with the neighbouring vortex pair on the left-hand side. The above simulation results are consistent with our discussion in §5 and §6. For fully developed two-dimensional vortex flow, Eckhaus instability plays an important role in the wavelength selection process and splitting and merging of vortices occur continuously.

8. Conclusion

Eckhaus instability was examined for the flow in channels with either curvature or rotation or both, using linear stability theory and spectral methods. The results explain several experimental phenomena. Curvature and rotation both cause similar instabilities with respect to spanwise perturbations in these geometries. The Eckhaus stable region was found to be a small closed region, different from any other periodic flow known to the authors. The stability criterion based on amplitude expansion given by Eckhaus (1965) does not always apply, even in the region close to Re_c. Outside the Eckhaus stable region, splitting and merging of vortex pairs occur and the spanwise wavenumbers are selected by the Eckhaus instability. Two pairs of vortices are split apart by a new pair to yield three pairs if the wavenumber of the vortices is small. If instead the wavenumber is large, the two pairs merge into one pair. Most experimentally observed wavenumbers are the ones which are least unstable to spanwise perturbations. At certain Re all vortices are equally unstable to spanwise perturbations and repetitive splitting and merging of vortex pairs occur. The wavenumber selection process as the flow proceeds downstream can be described as follows. Near the entrance of the channel, the flow is one-dimensional Poiseuille

type flow. Further downstream, vortices with spanwise wavenumber near those with maximum primary growth rate develop first. At these locations, the primary instability plays an important role in the wavenumber selection process. Further downstream, as the flow approaches fully developed two-dimensional vortex flow, the Eckhaus instability or wavy instability sets in, depending on which has dominant growth rate. When Re is not too high, the spanwise wavenumber of the flow lies in the Eckhaus valley, i.e. the region of low Eckhaus growth rate. When Re is very high, the stability of three-dimensional vortices must be examined to predict wavenumber selection.

The authors gratefully acknowledge the CPU time supplied by Myrias Inc. and the financial support of the Natural Sciences and Engineering Research Council of Canada.

REFERENCES

ALFREDSSON, P. A. & PERSSON, H. 1989 Instabilities in channel flow with system rotation. *J. Fluid Mech.* **202**, 543–557.

BENJAMIN, T. B. & FEIR, J. E. 1967 The disintegration of wave trains on deep water. Part 1. Theory. **27**, 417–430.

BIPPES, H. 1978 Experimental study of the laminar–turbulent transition of a concave wall in a parallel flow. *NASA TM.* 75243.

BLAND, S. B. & FINLAY, W. H. 1991 Transitions towards turbulence in a curved channel. *Phys. Fluids* A **3**, 106–114.

CANUTO, C., HUSSAINI, M. Y., QUARTERONI, A. & ZANG, T. A. 1988 *Spectral Methods in Fluid Dynamics.* Springer.

CLEVER, R. M. & BUSSE, F. H. 1974 Transition to time-dependent convection. *J. Fluid Mech.* **65**, 625–645.

DIPRIMA, R. C. & SWINNEY, H. L. 1985 Instabilities and transition in flow between concentric rotating cylinders. In *Hydrodynamic Instabilities and the Transition to Turbulence*, 2nd edn (ed. H. L. Swinney & J. P. Gollub), Topics in Applied Physics, vol. 45, pp. 139–180. Springer.

DOMINGUEZ-LERMA, M. A., CANNELL, D. S. & AHLER, G. 1986 Eckhaus boundary and wavenumber selection in Rotating Couette–Taylor flow. *Phys. Rev.* A **34**, 4956–4970.

ECKHAUS, W. 1965 *Studies in Nonlinear Stability Theory.* Springer.

FINLAY, W. H. 1990 Transition to oscillatory motion in rotating channel flow. *J. Fluid Mech.* **215**, 209–227.

FINLAY, W. H., KELLER, J. B. & FERZIGER, J. H. 1988 Instability and transition in curved channel flow. *J. Fluid Mech.* **194**, 417–456.

FOX, L. & PARKER, I. B. 1968 *Chebyshev Polynomials in Numerical Analysis.* Oxford University Press.

GARDNER, D. R., TROGDON, S. A. & DOUGLASS, R. W. 1989 A modified Tau spectral method that eliminates spurious eigenvalues. *J. Comp. Phys.* **80**, 133–167.

JONES, C. A. 1981 Nonlinear Taylor vortices and their stability. *J. Fluid Mech.* **157**, 135–162.

JONES, C. A. 1985 Numerical methods for the transition to wavy Taylor vortices. *J. Comp. Phys.* **61**, 321–344.

KELLEHER, M. D., FLENTIE, D. L. & MCKEE, R. J. 1980 An experimental study of the secondary flow in a curved rectangular channel. *Trans. ASME* I: *J. Fluids Engng.* **102**, 92–96.

LIGRANI, P., KENDALL, M. R. & LONGEST, J. E. 1990 Appearance, disappearance and spanwise wavenumber selection of Dean vortex pairs in a curved rectangular channel. *Phys. Fluids* A (Submitted).

LIGRANI, P. & NIVER, R. D. 1988 Flow visualization of Dean vortices in a curved channel with 40 to 1 aspect ratio. *Phys. Fluids* **31**, 3605–3618.

MASUDA, S. & MATSUBARA, M. 1989 Visual study of boundary layer transition on rotating flat plate *IUTAM Symp. on Laminar–Turbulent Transition.* Springer.

MATSSON, J. O. E. & ALFREDSSON, P. H. 1990 Curvature- and rotation-induced instabilities in channel flow. *J. Fluid Mech.* **202**, 543–557.

MEYER-SPASCHE, R. & KELLER, H. B. 1985 Some bifurcation diagrams for Taylor vortex flows. *Phys. Fluids* **28**, 1248–1252.

MOSER, R. D. & MOIN, P. 1984 Direct numerical simulation of curved turbulent channel flow. *NASA TM* 85974.

MOSER, R. D. & MOIN, P. 1987 The effects of curvature in wall-bounded turbulent flow. *J. Fluid Mech.* **175**, 497–510.

MOSER, R. D., MOIN, P. & LEONARD, A. 1983 A spectral numerical method for the Navier–Stokes equations with applications to Taylor–Couette flow. *J. Comp. Phys.* **52**, 524–544.

NAGATA, M. 1986 Bifurcations in Couette flow between almost corotating cylinders. *J. Fluid Mech.* **169**, 229–250.

NAGATA, M. 1988 On wavy instabilities of the Taylor-vortex flow between corotating cylinders. *J. Fluid Mech.* **188**, 585–598.

NAGATA, M. & BUSSE, F. H. 1983 Three-dimensional tertiary motion in a plane shear layer. *J. Fluid Mech.* **135**, 1–26.

PAAP, H. & RIECKE, H. 1990 Wave-number restriction and mode interaction in Taylor vortex flow: Appearance of a short-wavelength instability. *Phys. Rev.* A **41**, 1943–1951.

RIECKE, H. & PAAP, H. 1986 Stability and wave-vector restriction of axisymmetric Taylor vortex flow. *Phys. Rev.* A **33**, 547–553.

STUART, J. T. & DIPRIMA, R. C. 1978 The Eckhaus and Benjamin–Feir resonance mechanism. *Proc. R. Soc. Lond.* A **362**, 27–41.

TRITTON, D. J. & DAVIES, P. A. 1985 Instabilities in geophysical fluid dynamics. In *Hydrodynamic Instabilities and the Transition to Turbulence*, 2nd edn (ed. H. L. Swinney & J. P. Gollub), Topics in Applied Physics, vol. 45, pp. 229–270. Springer.

ZEBIB, A. 1984 A Chebyshev method for the solution of boundary value problems. *J. Comp. Phys.* **53**, 443–455.